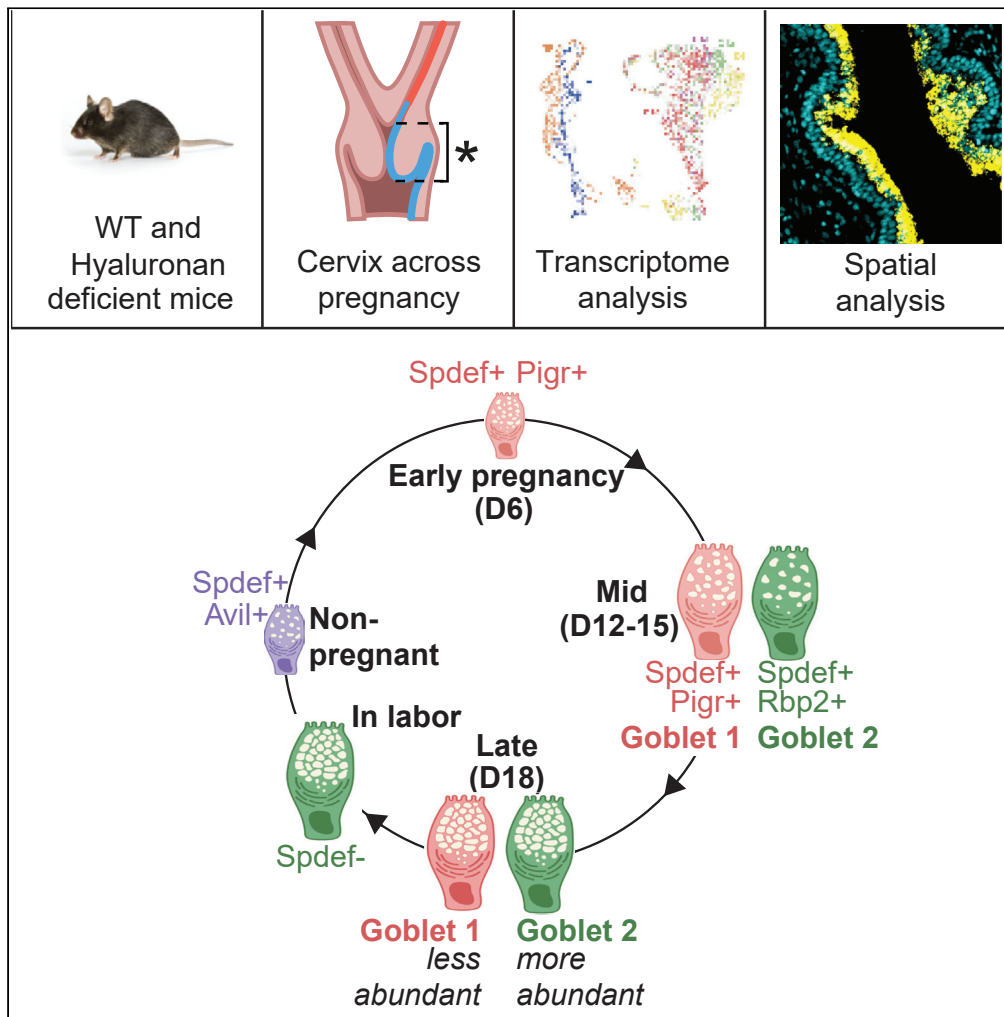


Article

# Dynamic states of cervical epithelia during pregnancy and epithelial barrier disruption



Anne Cooley,  
ShanmugaPriyaa  
Madhukaran,  
Elizabeth  
Stroebele, ...,  
Yucel Akgul, Gary  
C. Hon, Mala  
Mahendroo

gary.hon@utsouthwestern.edu  
(G.C.H.)  
mala.mahendroo@  
utsouthwestern.edu (M.M.)

Highlights

Mouse cervix single-cell  
analysis in non-  
pregnancy, pregnancy,  
and in labor

Cervix epithelia  
subpopulations display  
spatial and temporal  
specificity

Goblet cells are the  
dominant subtype in  
pregnancy and in labor

During labor,  
transcriptional reset  
expands non-pregnant  
epithelial populations

Cooley et al., iScience 26,  
105953  
February 17, 2023 © 2023 The  
Author(s).  
[https://doi.org/10.1016/  
j.isci.2023.105953](https://doi.org/10.1016/j.isci.2023.105953)



## Article

## Dynamic states of cervical epithelia during pregnancy and epithelial barrier disruption

Anne Cooley,<sup>1,5</sup> ShanmugaPriyaa Madhukaran,<sup>2,5</sup> Elizabeth Stroebele,<sup>1</sup> Mariano Colon Caraballo,<sup>2</sup> Lei Wang,<sup>1</sup> Yucel Akgul,<sup>4</sup> Gary C. Hon,<sup>1,2,3,\*</sup> and Mala Mahendroo<sup>1,2,6,\*</sup>

## SUMMARY

**The cervical epithelium undergoes changes in proliferation, differentiation, and function that are critical to ensure fertility and maintain pregnancy. Here, we identify cervical epithelial subtypes in non-pregnant, pregnant, and in labor mice using single-cell transcriptome and spatial analysis. We identify heterogeneous subpopulations of epithelia displaying spatial and temporal specificity. Notably in pregnancy, two goblet cell subtypes are present in the most luminal layers with one goblet population expanding earlier in pregnancy than the other goblet population. The goblet populations express novel protective factors and distinct mucosal networks. Single-cell analysis in a model of cervical epithelial barrier disruption indicates untimely basal cell proliferation precedes the expansion of goblet cells with diminished mucosal integrity. These data demonstrate how the cervical epithelium undergoes continuous remodeling to maintain dynamic states of homeostasis in pregnancy and labor, and provide a framework to understand perturbations in epithelial health that increase the risk of premature birth.**

## INTRODUCTION

Cervical epithelial cells have diverse roles during the non-pregnant (NP) reproductive cycle, throughout pregnancy, and parturition. These cells support fertility, provide a physical and immunological barrier to prevent the ascension of pathogens to the upper reproductive tract, and elicit signals that kill non-commensal pathogens.<sup>1</sup> Cervical epithelia carry out these functions in the context of a dynamic tissue that undergoes continuous remodeling before, during, and after pregnancy.<sup>2</sup>

Driven by the ovarian steroid hormones progesterone (P4) and estrogen (E2), cervical epithelia undergo numerous structural, morphological, and functional changes throughout the NP reproductive cycle. These hormones regulate proliferation, differentiation, mucus secretion, and the ability of epithelial cells to respond to pathogenic microbes.<sup>1</sup> As a key component of the mucosal immune system, vaginal and cervical epithelia produce mucins, cytokines, antimicrobial molecules, and transport immunoglobulins essential to protect the female reproductive tract from the invasion of pathogens.<sup>3,4</sup> The mucosal environment is finely balanced to provide pathogen surveillance and facilitate the migration of sperm from the cervicovaginal canal to the fallopian tube for fertilization.<sup>5–7</sup> Disruptions in the epithelial barrier can lead to sexually transmitted infections and/or infertility.<sup>8,9</sup>

Numerous studies report changes in the levels of cytokines, antimicrobial molecules, protease inhibitors, mucins, and immunoglobulins in cervicovaginal fluids/mucus plug of pregnant women relative to NP women, suggesting an alteration in epithelial subtypes or responses in the unique hormonal milieu of pregnancy.<sup>10–15</sup> Disruptions in the epithelial barrier or increased mucus permeability are associated with increased susceptibility to ascending infections and preterm birth in women. In mice, compromised epithelial barrier due to loss of hyaluronan, chemical disruption, or loss of the gel-forming mucin, Muc5b increases rates of ascending infection-mediated preterm birth.<sup>16–23</sup> Despite many efforts, effective therapies for prevention are lacking due to an incomplete understanding of the specialized epithelial subtypes in the cervix, their functions and their regulation throughout pregnancy and parturition. Hence, understanding the dynamic cell state changes during pregnancy is a prerequisite to comprehend the mechanism at play during normal and preterm cervical remodeling.

The cervical epithelia are divided into the endocervical and ectocervical regions (Figure 1A). The human endocervix consists of columnar and squamous epithelium and contains glands. The ectocervix is solely stratified squamous epithelium.<sup>24,25</sup> In mice, both regions contain stratified squamous epithelium and

<sup>1</sup>Cecil H. and Ida Green Center for Reproductive Biology Sciences, University of Texas Southwestern Medical Center, Dallas, TX 75390, USA

<sup>2</sup>Department of Obstetrics and Gynecology, University of Texas Southwestern Medical Center, Dallas, TX 75390, USA

<sup>3</sup>Department of Bioinformatics, University of Texas Southwestern Medical Center, Dallas, TX 75390, USA

<sup>4</sup>Department of Plastic Surgery, University of Texas Southwestern Medical Center, Dallas, TX 75390, USA

<sup>5</sup>These authors contributed equally

<sup>6</sup>Lead contact

\*Correspondence:

[gary.hon@utsouthwestern.edu](mailto:gary.hon@utsouthwestern.edu) (G.C.H.),

[mala.mahendroo@](mailto:mala.mahendroo@utsouthwestern.edu)

[utsouthwestern.edu](mailto:utsouthwestern.edu) (M.M.)

<https://doi.org/10.1016/j.isci.2023.105953>



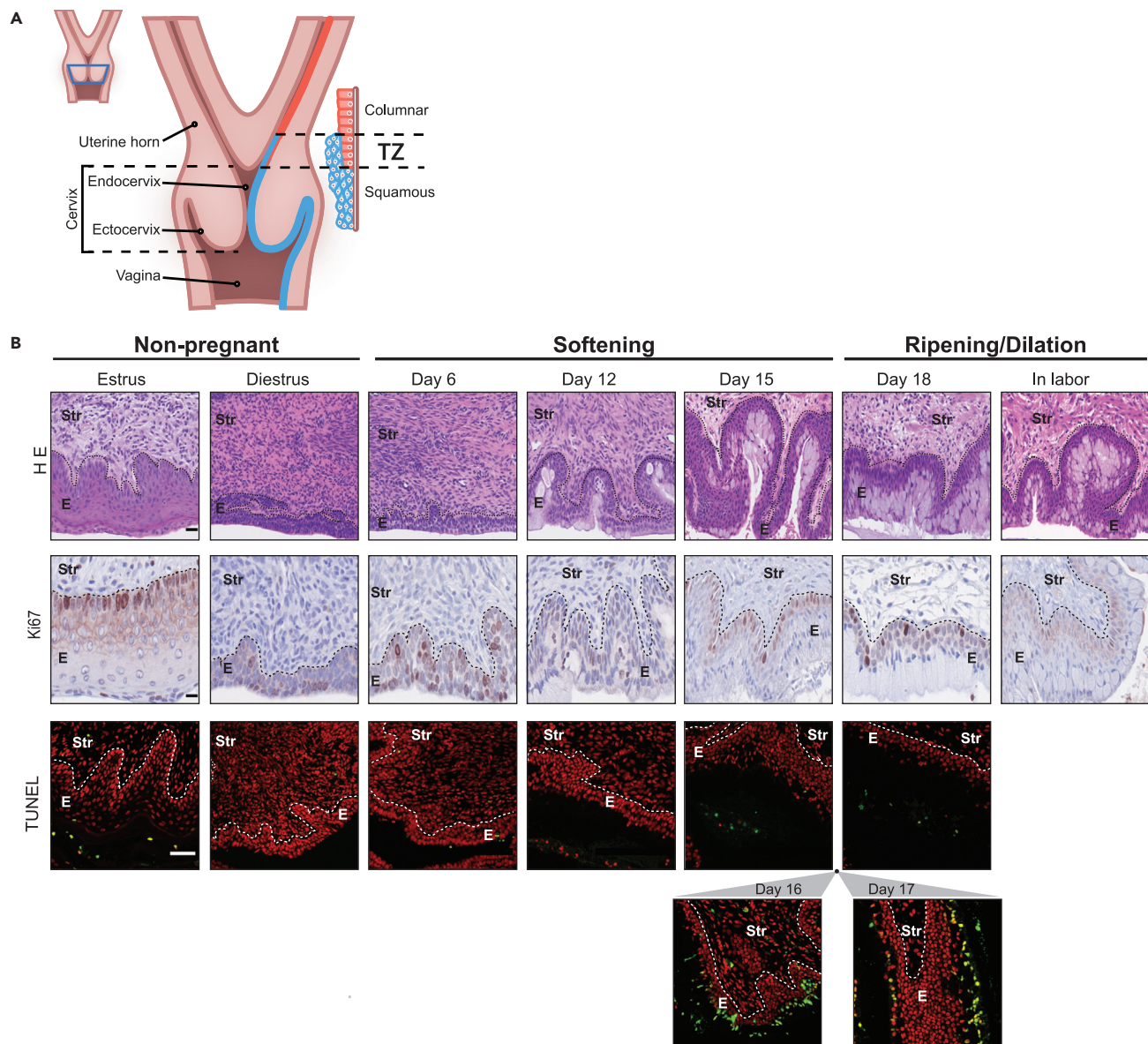


**Figure 1. Morphological changes in cervical epithelia during pregnancy**

(A) Schematic longitudinal section of mouse uterus and cervix. Blue: stratified squamous epithelia of endo- and ectocervix. Red: columnar epithelium of uterus. Transition zone (TZ): Boundary comprising both types of epithelia. Blue boxed area: Indicates cervical region below TZ collected for single-cell libraries.

(B) Morphological changes in cervical epithelia in non-pregnant, pregnant (GD6, GD12, GD15, and GD18), and in labor mice. Shown are H&E staining (top), Ki67 immunostaining for proliferation (middle), and TUNEL staining for cell death (bottom) (red: nuclei, green: TUNEL<sup>+</sup>). E: Epithelia; Str: Stroma. Scale bar 50  $\mu$ m. Representative images from three independent samples per each group.

lack glands.<sup>26–31</sup> The mouse endocervix also contains columnar epithelium though abundance varies during development and the estrus cycle.<sup>32</sup> Despite potential differences in endocervical epithelial subtypes between mice and humans, both produce a similar mucus network and are fortified with a similar arsenal of protective factors.<sup>33–35</sup> For example, proteomic analysis of human cervicovaginal mucus in pregnancy identifies the gel-forming mucins Muc5b and Muc5ac and a recent assessment of mice with a null mutation in Muc5b demonstrates their increased rate of preterm birth with exposure to an ascending infection.<sup>14,23</sup>

The focus of this study is to identify cervical epithelial subtypes in the cervix of non-pregnant and pregnant mice and to evaluate their spatial location in the endo- and ectocervix. Here, we identify transcriptional cell

states of the cervical epithelia at four gestational time points over the 19-day mouse pregnancy relative to the cervix of in labor (IL) and NP mice. Using single-cell genomics and localization analysis, we define dynamic changes in cell states that begin in early pregnancy. We identify a misregulation in cell state transition associated with a mouse model of epithelial barrier disruption with increased susceptibility to ascending infection-induced preterm birth.

## RESULTS

### Morphological changes in cervical epithelia during pregnancy

The multilayered stratified epithelium undergoes marked changes in proliferation, differentiation, and apoptosis throughout the NP estrus cycle and 19-day pregnancy (Figures 1B and S1).<sup>36,37</sup> Most notable during pregnancy is the increase in secretory epithelia that peaks in cell size and cell number on gestation day 18 (GD18) and IL, as seen by H&E staining (Figure 1B). Proliferative (Ki67<sup>+</sup>) cells are present in all layers of epithelia on GD6 and 12, yet are confined primarily to the basal layers on GD15, GD18, and IL. The presence of a few TUNEL<sup>+</sup> cells (green) in the most luminal layers on gestation day 15 and 18 indicates cell death occurs in late pregnancy. Assessment of gestation day 16 and 17 time points identifies these time points as a peak of cell death in the luminal layers of the endocervix that declines on d18. During pregnancy, cell morphology and proliferation are similar between the endo- and ectocervix while cell death occurs primarily in the endocervix. In contrast, during the NP diestrus stage, secretory epithelia are abundant in the ecto- but not the endocervix (Figure S1). These observations highlight the dynamic structural and compositional reorganization of cervical epithelia during pregnancy.

### Remodeling of cervical epithelia is associated with alterations in transcriptional and open chromatin status

To spatially demarcate the endocervix, the uterine epithelia, and the boundary between the endocervix and uterus termed the transition zone (TZ),<sup>25</sup> we performed immunofluorescence (IF) imaging for markers of squamous basal cells (keratin 5) and columnar epithelia (keratin 8) in the NP proliferative (estrus) and secretory (diestrus) stages (Figures S2 and S3). The endocervix region was defined by the absence of glands and the presence of squamous Krt5<sup>+</sup> cells (estrus Figure S2) or Krt5<sup>+</sup> and Krt8<sup>+</sup> cells (diestrus, Figure S3). The uterine region was defined by the presence of Krt8<sup>+</sup> cells in both luminal and glandular epithelium. The TZ where columnar and squamous epithelia overlap was identified just below the uterine region, thus defining the boundary between the endocervix and uterus and as previously described.<sup>27,31,32</sup>

To define the dynamic transcriptional states of cervical epithelia, we performed time-course single-cell RNA sequencing (scRNA seq). Mouse cervical tissue was separated from the uterus just below the TZ (Figure 1A, blue box) and harvested for scRNA-Seq library preparation using cell digestion methods optimized to ensure epithelial cell viability. The NP library consists of cells pooled from the secretory (diestrus) and proliferative (estrus) stages of the cycle. To generate the pregnancy libraries, time points in pregnancy were selected to span the phases of cervical softening, ripening, and day 19 in labor after delivery of 1–2 pups (Figure 2A). Based on cervical weight which can vary from 8 mg in NP to 30 mg in labor due to increased cell proliferation and tissue hydration,<sup>38</sup> varying numbers of cervixes were pooled to obtain a sufficient number of single cells for library preparation. Cervixes were pooled from the indicated number of mice: NP (n = 9; 7 diestrus and 2 estrus), GD6 (n = 5), GD12 (n = 4), GD15 (n = 3), GD18 (n = 3), and IL (n = 3). After stringent quality control filters (see STAR Methods and Table S1), we recovered 26,493 high-quality cells across the six time points. Epithelial cells were the main cell type recovered at most time points while the number of non-epithelial cells captured was low relative to their abundance in tissue (Figure 2A). The gestation day 6 library had a more diverse representation of cell types, likely due to better cell dispersion efficiency in that library. The dominance of epithelia in single-cell libraries is also observed in another study.<sup>39</sup> Clustering of all time points showed five distinct cell types that were captured from the cervical tissue: epithelial (Epcam<sup>+</sup>, Ehf<sup>+</sup>), immune (Tyrobp<sup>+</sup>), endothelial (Pecam1<sup>+</sup>), stromal (Col1a2<sup>+</sup>), and red blood cells (Hbb-bt<sup>+</sup>) (Figures 2B and 2C).<sup>40</sup> The expression of additional cell type-specific genes also confirms the identification of the cell types (Figure 2D). Since epithelial cells were the dominant cell type captured at each time point, we focused subsequent analyses on characterizing how epithelial cell states change throughout pregnancy.

To define the open chromatin status of cervical cell types, we also performed single-cell ATAC-Seq<sup>41</sup> throughout pregnancy time points. We recovered 30,758 nuclei (Figure 2E) that represent multiple cell types of the cervix with distinct open chromatin profiles (Figure 2F). We annotated each cluster by

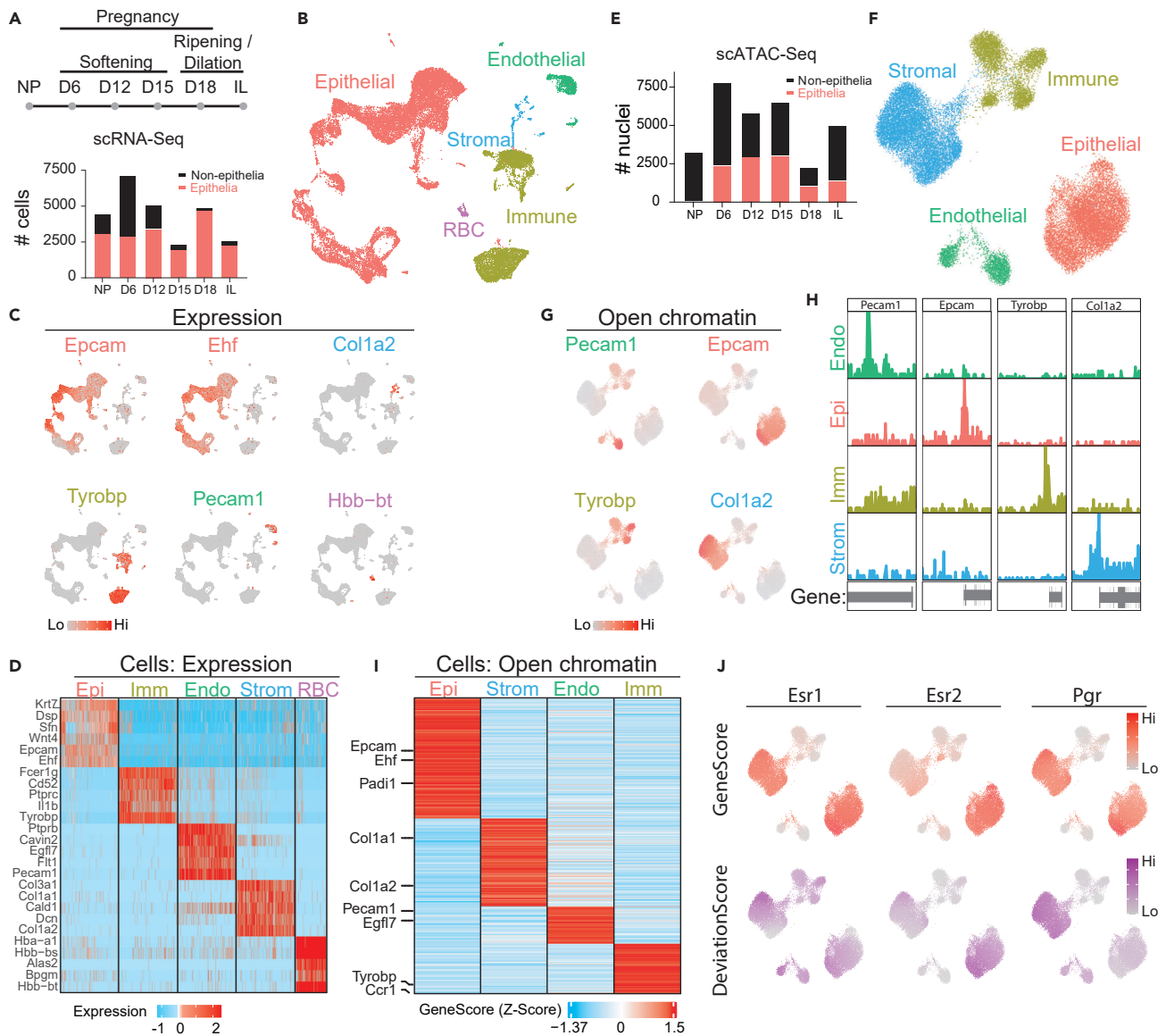


**Figure 2. Remodeling of cervical epithelia is associated with alterations in transcriptional and open chromatin status**

(A) (top) Design of scRNA-Seq experiments (gray circles: sequencing time points). (bottom) Distribution of epithelia and non-epithelial cells captured per time point. Each time point is a single replicate.

(B) UMAP visualization of all cells captured from all time points of scRNA-Seq.

(C) Feature plots indicate the expression of genes used to identify different cell types. Epcam and Ehf: epithelia; Col1a2: stroma; Tyrobp: immune; Pecam1: endothelia, and Hbb-bt: red blood cells.

(D) Heatmap showing the expression of cell type-specific genes.

(E) Distribution of epithelia and non-epithelial cells captured per time point of scATAC-Seq. Each time point is a single replicate.

(F) UMAP visualization of all cells captured from all time points of scATAC-Seq.

(G) Feature plots indicate the open chromatin status of genes used to identify different cell types.

(H) Genome browser snapshots of open chromatin status for the genes in (G), for each cell type.

(I) Heatmap showing the cell type-specific open chromatin status of genes.

(J) (top) Feature plot of open chromatin status for Esr1, Esr2, and Pgr. (bottom) Motif deviation scores for these transcription factors indicate cell type-specific enrichment of TF-binding motifs at open chromatin regions.

examining the open chromatin status for cell type specifically expressed genes: epithelial (Epcam<sup>+</sup>), immune (Tyrobp<sup>+</sup>), endothelial (Pecam1<sup>+</sup>), and stromal (Col1a2<sup>+</sup>) (Figures 2G and 2H). The open chromatin status of additional cell type specifically expressed genes also confirms these annotations (Figure 2I).

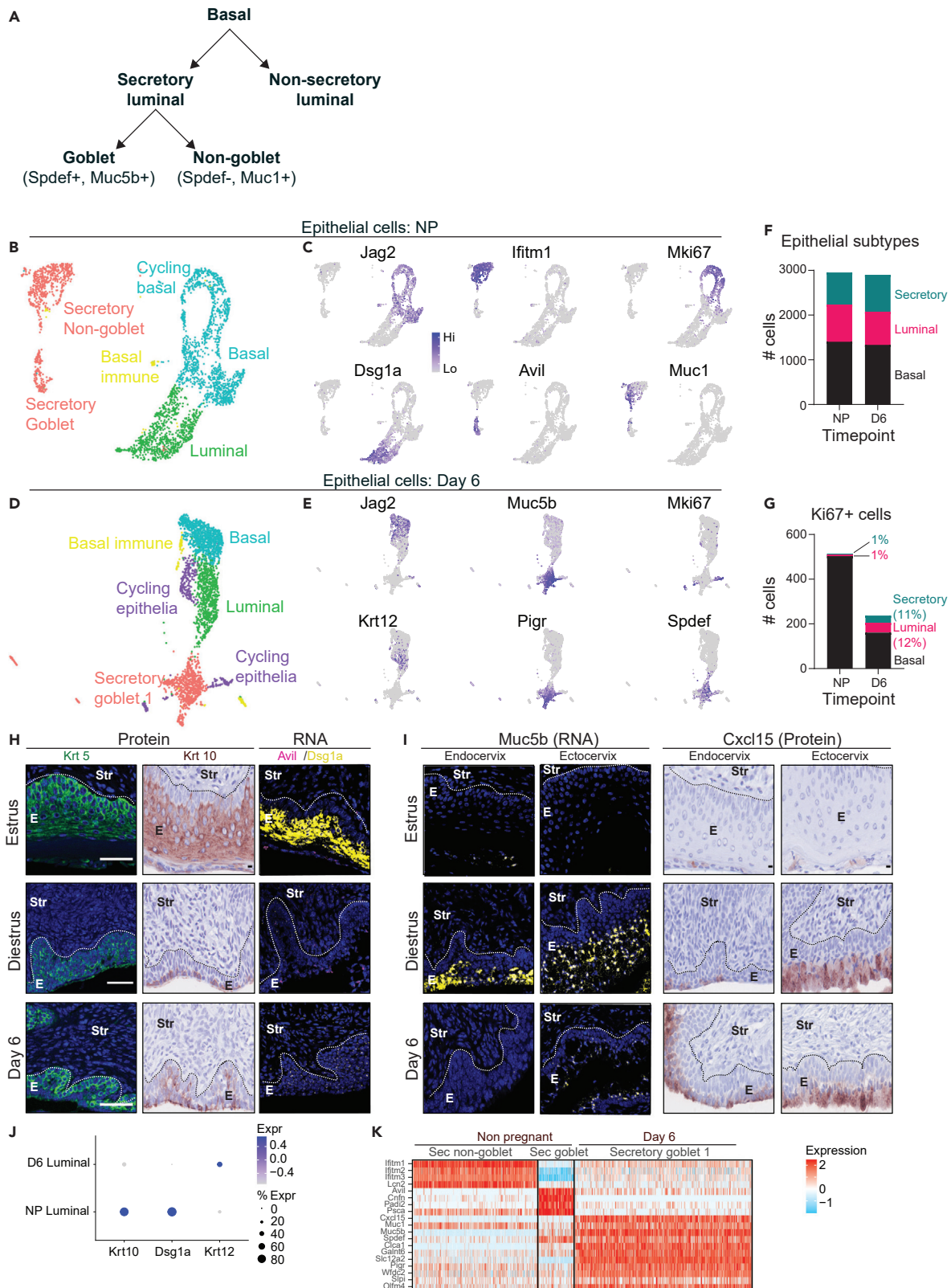


**Figure 3. Shifts in epithelial subtypes and proliferation in early softening**

- (A) Schematic of lineage relationships of cervical epithelial cell types. Basal cells give rise to luminal non-secretory and luminal secretory cells. Luminal secretory cells can mature into non-goblet (Spdef<sup>-</sup> Muc1<sup>+</sup>) or goblet cells (Spdef<sup>+</sup>, Muc5b<sup>+</sup>).
- (B) UMAP visualization of epithelial cells from the non-pregnant time point with three major types of epithelia: basal, luminal, and secretory.
- (C) Feature plots showing the expression of genes differentially expressed between the NP epithelia. Jag2: basal cells; Mki67: cycling basal cells; Dsg1a: luminal cells; Ifitm1, Avil, and Muc1: secretory cells.
- (D) UMAP visualization of epithelial cells from GD6.
- (E) Feature plots showing the expression of genes differentially expressed between the different types of GD6 epithelia. Jag2: basal cells; Mki67: cycling basal cells; Krt12: luminal cells; Muc5b, Pigr, and Spdef: secretory cells.
- (F) Bar chart quantifying epithelial subtypes in NP and GD6. Each time point is a single replicate.
- (G) Bar chart quantifying proliferating (Mki67<sup>+</sup>) epithelial cells in NP and GD6.
- (H) IF and IHC showing protein expression of Krt5 (green), and Krt10 (brown) in mouse endocervical epithelia from NP (estrus and diestrus) and GD6. Krt5: basal cells; Krt10: luminal epithelia. RNAscope analysis of Dsg1a (yellow) with Avil (pink) mRNA in mouse endocervical epithelia from NP and GD6. DAPI (blue): nuclei. E: Epithelia; Str: Stroma. Scale bar 50  $\mu$ m, objective lens 40 $\times$ . Representative images from two independent samples per group.
- (I) Expression of Muc5b (yellow) mRNA by RNAscope and Cxcl15 (brown) protein by IHC in mouse endo and ectocervical epithelia from NP (estrus and diestrus) and GD6. DAPI: nuclei. E: Epithelia; Str: Stroma. Representative images from three independent samples per group.
- (J) Dot plot showing the expression of luminal markers.
- (K) Heatmap highlighting the different genes expressed in secretory clusters from NP and GD6.

Finally, by examining the enrichment of motifs at open chromatin peaks, we can identify transcription factors with potential roles in regulating specific cell types during cervical remodeling.<sup>42</sup> This analysis suggests divergent roles for well-known nuclear hormone receptors. For example, estrogen receptor 1 (Esr1) is active (gene expression and enriched open chromatin for the binding site) in both stromal and epithelial cells, while Esr2 appears more active in epithelial cells as compared to stroma (Figure 2J).

**Shifts in epithelial subtypes and proliferation in early softening**

The squamous epithelium can be subdivided into basal and luminal cells based on specific markers (Figure 3A). Basal cell markers include Krt5, Krt14, Trp63, and cell cycle genes.<sup>43,44</sup> Luminal cells can be further subdivided into non-secretory luminal subtypes (e.g. Dsg1a<sup>+</sup>, keratinocyte) and secretory luminal cells (defined as cells expressing mucin genes). Secretory luminal cells are further partitioned into goblet cells, a specialized cell that synthesizes gel-forming mucins (e.g. Muc5b) and non-goblet secretory cells which make transmembrane mucins (e.g. Muc1). Using established markers that distinguish subtypes, we sought to examine at a higher resolution the epithelial subtypes and their cell state transitions that occur in the early softening period, by comparing epithelial subtypes in NP and GD6.

Basal, luminal, and secretory clusters in NP and GD6 samples (Figures 3B and 3D) had a similar distribution of cell types (Figure 3F). Clustering of these two datasets separately (Figures 3B and 3D) or together (Figure S4) demonstrates distinct clustering and features of subtypes between NP and D6. Notably, we observed an increase in proliferating (Ki67<sup>+</sup>) non-basal cells on GD6 compared to NP (Figures 3C, 3E, and 3G). We also observed changes in luminal markers over time, with Dsg1a specifically marking non-secretory luminal cells in NP and Krt12 specifically marking non-secretory luminal cells in D6 (Figures 3C, 3E, and S5). Krt12 has not previously been described in the cervix and is considered a marker of the differentiated epithelium of the cornea.<sup>45</sup>

In NP, we identified two secretory clusters expressing mucin 1 (Muc1) that were distinguished by the markers Ifitm1 (Interferon-induced transmembrane protein 1) and Avil (Advillin) (Figure 3C). In contrast, on GD6, we identified only one secretory population (Muc5b<sup>+</sup>, Pigr<sup>+</sup>). The GD6 secretory cluster and the NP Avil<sup>+</sup> cluster expressed the transcription factor Spdef which is required for the differentiation of goblet cells.<sup>46,47</sup> Goblet cells have been described in the NP cervix.<sup>34</sup> Fluorescent microscopic analysis of protein or RNA expression for basal (Krt5<sup>+</sup>), luminal (Krt10<sup>+</sup>/Dsg1a<sup>+</sup>), and secretory (Avil<sup>+</sup>/Muc5b<sup>+</sup>/Cxcl15<sup>+</sup>) markers confirms a shift in luminal subtypes from NP to GD6 (endocervix, Figures 3H and 3I). In the NP estrus stage, Krt10<sup>+</sup>/Dsg1a<sup>+</sup> luminal cells are abundant (Figure 3H) while in the NP diestrus stage Avil<sup>+</sup>/Muc5b<sup>+</sup>/Cxcl15<sup>+</sup> secretory luminal cells are abundant (Figure 3I). Avil<sup>+</sup> secretory cells are visible in the endocervical luminal layers in diestrus, with fewer Avil<sup>+</sup> cells in estrus and on GD6. Furthermore, during NP diestrus and GD6, we observe that goblet secretory cell expansion is similar in both the ectocervix and the endocervix as indicated by Muc5b and Cxcl15 expression (Figure 3I). Cxcl15 is a chemokine expressed in numerous mucosal and endocrine organs and is a specific marker of glandular but not luminal epithelia of the uterus.<sup>48,49</sup> Comparison of spatial expression of the above markers was similar between the endo- and ectocervix as shown in the complete panel NP and pregnancy time points (Figures S6–S8). The presence of distinct luminal subtypes in NP and GD6 is indicated

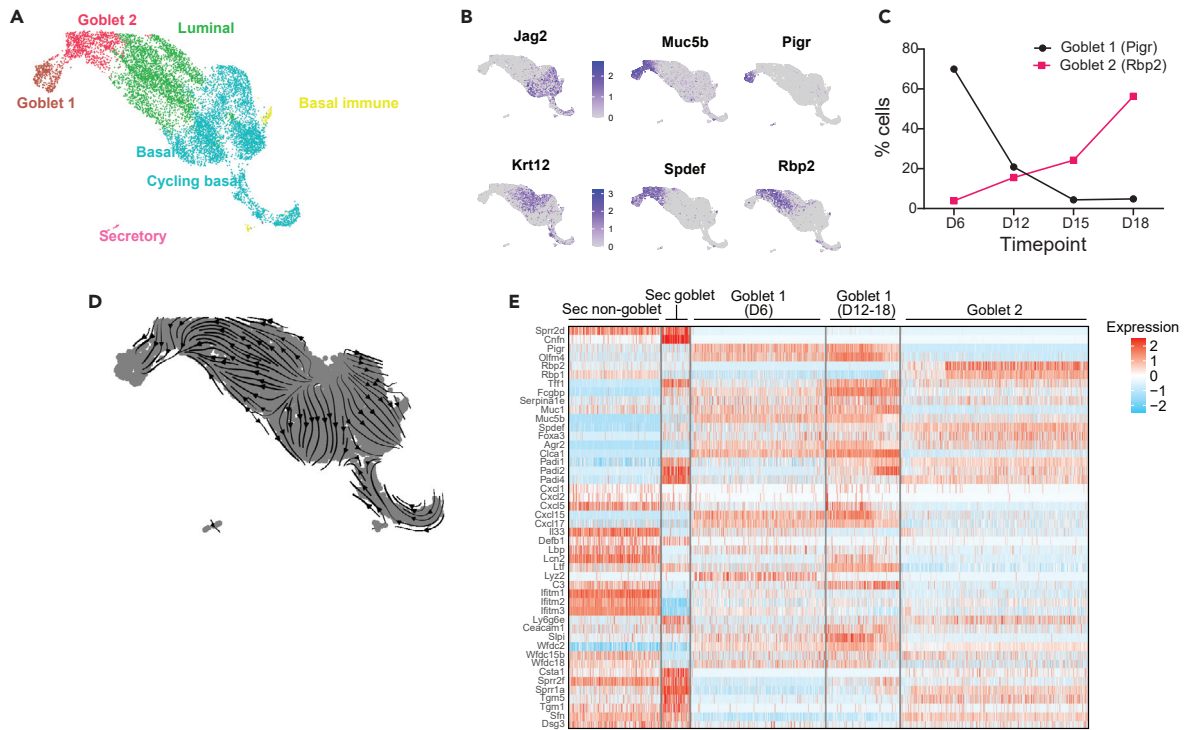


**Figure 4. Distinct populations of secretory cells during pregnancy**

(A) UMAP visualization of epithelial cells from GD12, GD15, and GD18.  
 (B) Feature plots show the markers used to identify the different epithelia clusters.  
 (C) Abundance of goblet subtypes shift between early pregnancy to late pregnancy in scRNA-Seq libraries. Pigr<sup>+</sup> goblet cells are at their highest level in GD6. Rbp2<sup>+</sup> goblet cells peak at GD18. Each time point is a single replicate.  
 (D) RNA velocity of the GD12-18 clustering shows strong directionality from luminal cells to Rbp2<sup>+</sup> goblet cells, but not to Pigr<sup>+</sup> goblet cells.  
 (E) Heatmap highlighting changes in gene expression across the different secretory clusters identified in the NP (Sec non-goblet and Sec-goblet) and GD6-18 clustering (Goblet 1 and Goblet 2).  
 (F) Spatial analysis of cervical epithelia subtype markers at GD6-18. Basal (Krt5), luminal (Krt10 and Krt12), goblet (Spdef, Muc5b, Muc1, Pigr, and Rbp2). Detection of Krt5 (green) and Krt 10 (brown) protein by IF and IHC. Detection of Krt12, Muc5b (yellow); Pigr, Muc1 (green); Spdef (teal blue) and Rbp2 (red) by RNAscope. DAPI(blue)-nuclei. In contrast to basal/luminal markers, expression of Spdef, Pigr, Rbp2, Muc5b, and Muc1 is restricted to cells close to the lumen. E: Epithelia, Str: Stroma; Scale bar 50  $\mu$ m, objective lens 40 $\times$ . Representative images from three independent samples per group.  
 (G) RNAscope images showing co-analysis of Spdef (pink) with Pigr or Rbp2 (yellow) mRNA in mouse endocervical epithelia from GD15. DAPI (gray)-nuclei. E: Epithelia; Str: Stroma. Scale bar 50  $\mu$ m, objective lens 40 $\times$ . Representative images from two independent samples per group.

in the dot plot (Figure 3J) and the secretory clusters in Figure 3K. Collectively, these data indicate two secretory populations in the NP cervix, one of which is an Avil<sup>+</sup>/Spdef<sup>+</sup>/Muc5b<sup>+</sup>/Muc1<sup>+</sup> goblet cell and the other is (Ifitm1<sup>+</sup> and Muc1<sup>+</sup>) (Figure 3K). On GD6, a single secretory goblet cell population (Secretory Goblet 1) is identified that is transcriptionally distinct from the NP goblet cell.

**Distinct populations of secretory cells during pregnancy**

We next examined epithelial subpopulation dynamics through cluster analysis of single-cell data from pregnancy time points GD12, GD15, and GD18 (Figure 4A). Cluster analysis identifies two populations of Muc5b<sup>+</sup>/Spdef<sup>+</sup> goblet cells: Goblet 1 cells express Pigr while Goblet 2 cells express Rbp2 (Figures 4B and Table S2). A comparison of goblet subtype abundance across the 4 pregnancy time points identifies Goblet 1 cells as most abundant in the scRNA-Seq library on GD6 and gradual decline toward GD18, while goblet 2 cells are rare in the earlier time points and peak in the GD18 library (Figure 4C). RNA velocity analysis of GD12, 15, and 18 libraries suggests luminal cells give rise to goblet 2 cells but not goblet 1 cells (Figure 4D). Luminal and goblet 2 cells express Rbp2 (Figure 4B), while goblet 1 does not. RNA velocity analysis does not indicate that goblet 1 cells arise from any other sequenced cells. We also identified a minor secretory cluster with the expression of Krt8/18 and Pigr but lacking the goblet markers Spdef and Muc5b. This cluster also uniquely expresses Prap1, Napsa, C3, and Gpx3 (Figure S9A) and shares transcriptional similarity to the glandular and luminal epithelia of the uterus.<sup>50</sup>

To further compare the major secretory clusters identified in the NP and gestation days 6, 12, 15, and 18, we examined the expression status of genes relevant to cervical epithelial function (Figure 4E). This analysis revealed temporal and functional distinctions in secretory cell populations. Notably, the two pregnancy-specific goblet populations are distinct from each other and distinct from the NP goblet and non-goblet secretory cluster. Goblet 1 uniquely expressed olfactomedin 4, Olfm4<sup>51-53</sup>; the chemokines, Cxcl15, Cxcl17, the calcium-activated chloride channel, Clca1 and the protease inhibitors, secretory leukocyte peptidase inhibitor (Slpi), and WAP four disulfide core domain 2 (Wfdc2). Goblet 2 lacks Muc 1 expression and expresses keratinocyte markers (Sprr2f, Sprr2a, Tgm5, and Sfn). We next evaluated the temporal patterns of goblet 1 and goblet 2 cells in the endocervix (Figure 4F) and spatial patterns between the endocervix and ectocervix (Figures S6-S8). Krt5 and Krt10/Krt12 identify basal and non-secretory luminal cells, respectively. Spdef marks both goblet 1 and goblet 2, while Pigr marks goblet 1 and Rbp2 marks goblet 2. Transcripts encoding Spdef were evident in the most luminal cell layers on GD12, 15, and 18, with the greatest number of Spdef<sup>+</sup> cells on GD18. Expression of Spdef on GD6 was below the detection level for RNAscope. The strong expression of Pigr and Rbp2 on GD15 prevented the identification of goblet cells expressing only Pigr or Rbp2. As seen in Figure 4G, numerous Spdef<sup>+</sup>Pigr<sup>+</sup> goblet 1 cells are identified with relatively few Spdef<sup>+</sup>Rbp2<sup>+</sup> goblet cells. A similar pattern is noted on GD18 (Figure S9B). Muc5b was highly expressed in the luminal layers on GD12 and GD15 with lower levels on GD6 and GD18. Muc1 transcripts were evident on days GD6, GD12, and GD15. The expansion of goblet cells in pregnancy occurs to a similar extent in both the endo- and ectocervix as seen in Figure S8.

**Goblet cell expansion in mid-late pregnancy is followed by induction of epithelial transcription programs in labor to repopulate NP-specific subtypes following birth**

To further examine epithelial cell dynamics, we expanded our analysis across NP, pregnant, and IL samples. Unexpectedly, clustering analysis shows that epithelial cells from IL samples clustered with NP rather than

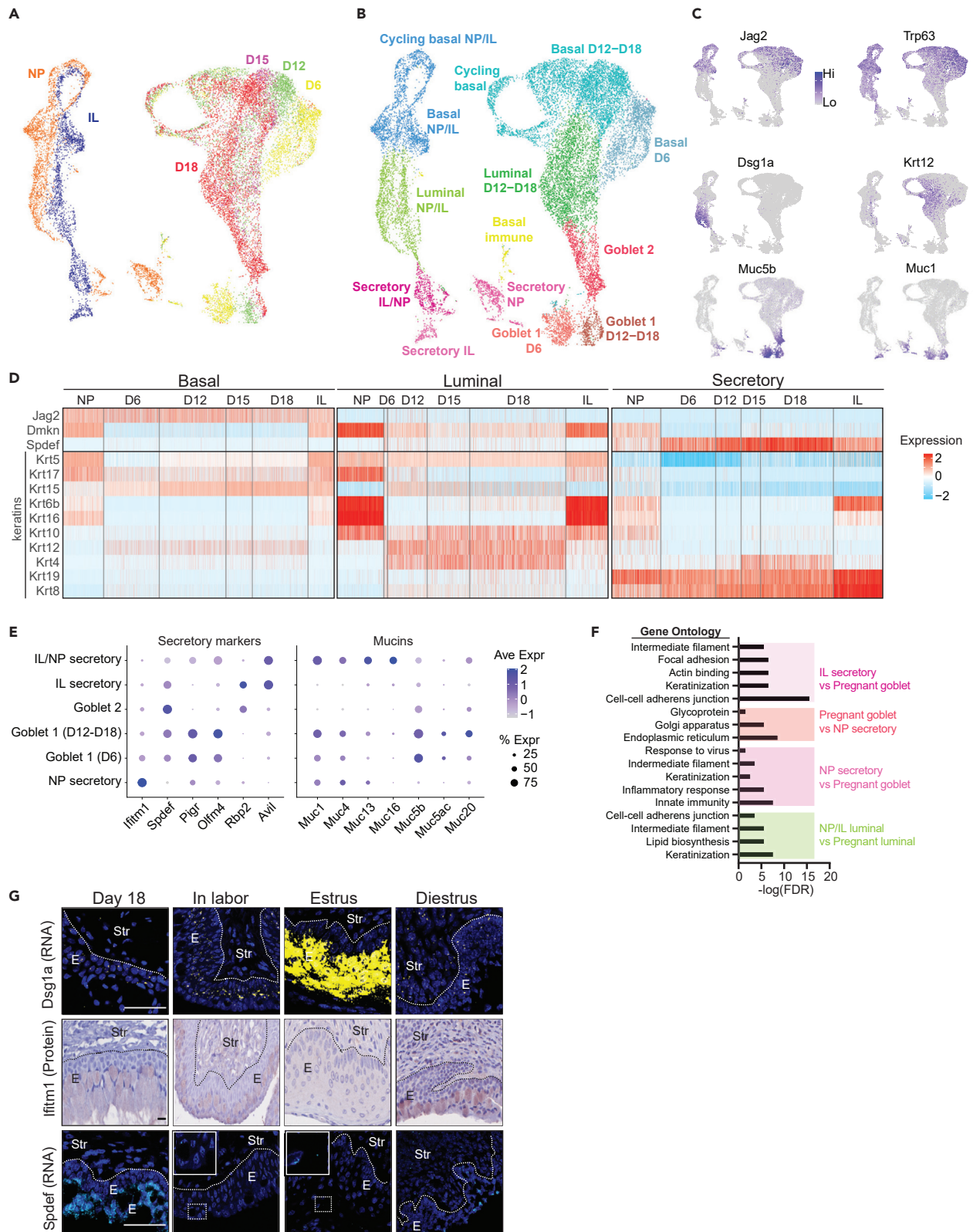


**Figure 5. Goblet cell expansion in mid-late pregnancy is followed by induction of epithelial transcription programs in labor to repopulate NP-specific subtypes following birth**

- (A) UMAP visualization of epithelia from all time points. Cells are colored by time point.  
 (B) As in (A), but cells are colored by epithelial type.  
 (C) Feature plots showing the expression of genes that identify epithelial subtypes.  
 (D) Heatmap highlighting temporal and subtype-specific changes in keratin gene expression from basal to luminal to secretory populations across pregnancy.  
 (E) Dotplots showing the expression of secretory markers and mucins in the different secretory clusters.  
 (F) Gene Ontology analysis highlights the functional changes in the luminal and secretory populations.  
 (G) Detection of *Dsg1a* (yellow) and *Spdef* (teal blue) mRNA expression by RNAscope and *Ifitm1* (brown) protein expression by IHC on GD18, IL, and NP (estrus and diestrus). DAPI (blue) - nuclei. Inserts show a magnified view of selected areas. E: Epithelia; Str: Stroma. Scale bar 50  $\mu$ m, objective lens 40 $\times$ . Representative images from two independent samples per group.

the pregnancy time points (Figure 5A). Basal and luminal cells were most concordant between the NP and IL (Figure 5B). Secretory cells were more divergent, with one cluster specific to NP, one specific to IL, and one shared. Among pregnancy time points, the goblet 1 cells clustered distinctly from the other time points and other clusters. While basal/luminal clusters had common markers (e.g. *Jag2* and *Trp63*) in all the time points, both secretory (*Muc5b* and *Muc1*) and non-secretory (*Dsg1a* and *Krt12*) clusters were distinct between NP/IL and pregnancy time points GD 6/12/15/18 (Figures 5C and Table S3). Analysis of keratin expression patterns (intermediate filament proteins with epithelial subtype specificity) further highlights the temporal shifts in subtype specificity from NP to pregnancy to IL (Figure 5D). Keratin expression and Gene Ontology pathways suggest that the transition to IL induces a transcriptional program similar to the NP-like state (Figures 5D–5F). The expression of secretory markers and mucin genes (Figure 5E) also highlights the temporal change in secretory cell populations and the type of mucins in cervical mucus. A previously unappreciated diversity of antimicrobial proteins (*Defensin B1* and small proline-rich proteins 1 and 2) and protease inhibitors (*Slpi*, *Wfdc2*, *Wfdc15b*, *Wfdc18*, *Spink 5*, and *Spink 12*) were identified with distinct temporal and subtype expression patterns (Figure S10). The transcriptional similarities identified between NP and IL epithelial subtypes in the single-cell data were supported by spatial analysis of luminal/secretory markers. RNA (*Dsg1a*, *Spdef*) and protein (*Ifitm1*) analysis demonstrate increased *Dsg1a*<sup>+</sup> cells in the intermediate luminal layers IL relative to D18 in the endo- and ectocervix (Figures 5G and S7). Upon completion of parturition, rodents immediately transition to the estrus stage of the NP cycle.<sup>54–56</sup> *Dsg1a* marks a luminal population of cells that are abundant in the estrus phase of the NP cycle. Protein staining for *Ifitm1* is evident in the IL secretory cells though at reduced levels compared to the NP diestrus secretory phase. Goblet cells present in the most luminal layers of epithelia in the IL are terminally differentiated as demonstrated by the downregulation of *Spdef* relative to GD18.

**Altered cell transition states characterize epithelial barrier disruption**

The cervical epithelia maintain a physical and immune barrier that is established as the first line of defense against opportunistic pathogens and other environmental insults.<sup>1,57,58</sup> During pregnancy, disruption of the physical barrier or mucosal immunity as demonstrated in numerous studies results in an increased risk of preterm birth due to an ascending infection.<sup>14,20,21,23</sup> Our analysis identifies a pregnancy-specific expansion of luminal epithelial subtypes, including two distinct goblet populations. Next, we use these findings as a reference to define the dysregulation of epithelial barrier function in mice lacking the glycosaminoglycan, hyaluronan (HA). Targeted loss of three genes (*Has1*, *Has2*, and *Has3*) encoding hyaluronan synthase (HAKO) in the cervix results in a morphologically disrupted secretory epithelium (Figure 6A), reduced cell death in luminal layers on GD16 and GD17 (Figure 6B), increased susceptibility to ascending infection as demonstrated by the presence of bacteria in the uterus of HAKO but not wild-type controls and a resulting increased expression of inflammatory genes within the uterus, placenta, and fetal membranes (Figures 6C–6E), and premature birth.<sup>20</sup> Hyaluronan synthesis is increased in the human cervix during pregnancy and pathogen-mediated breakdown of HA is associated with preterm birth, thus defining how HA protects epithelial cell function is warranted.<sup>59,60</sup> To examine how HA disruption alters epithelial cell state, we performed scRNA-Seq on HAKO mice at GD15 and GD18, when cervical HA synthesis is greatest.<sup>20,61</sup>

We observed that most cervical epithelial cells from HAKO mice clustered distinctly from wild-type (WT) mice (Figure 7A), with the exception of goblet cluster 1 (Figure 7B). Next, we examined the molecular differences between the WT and HAKO epithelial subtypes. We did not observe dramatic differences in the percentage of cells expressing characteristic marker genes for basal, luminal, and goblet cells (Figures 7C and 7D). In contrast, a small increase in the average level of *Krt5* expression was noted in the HAKO basal

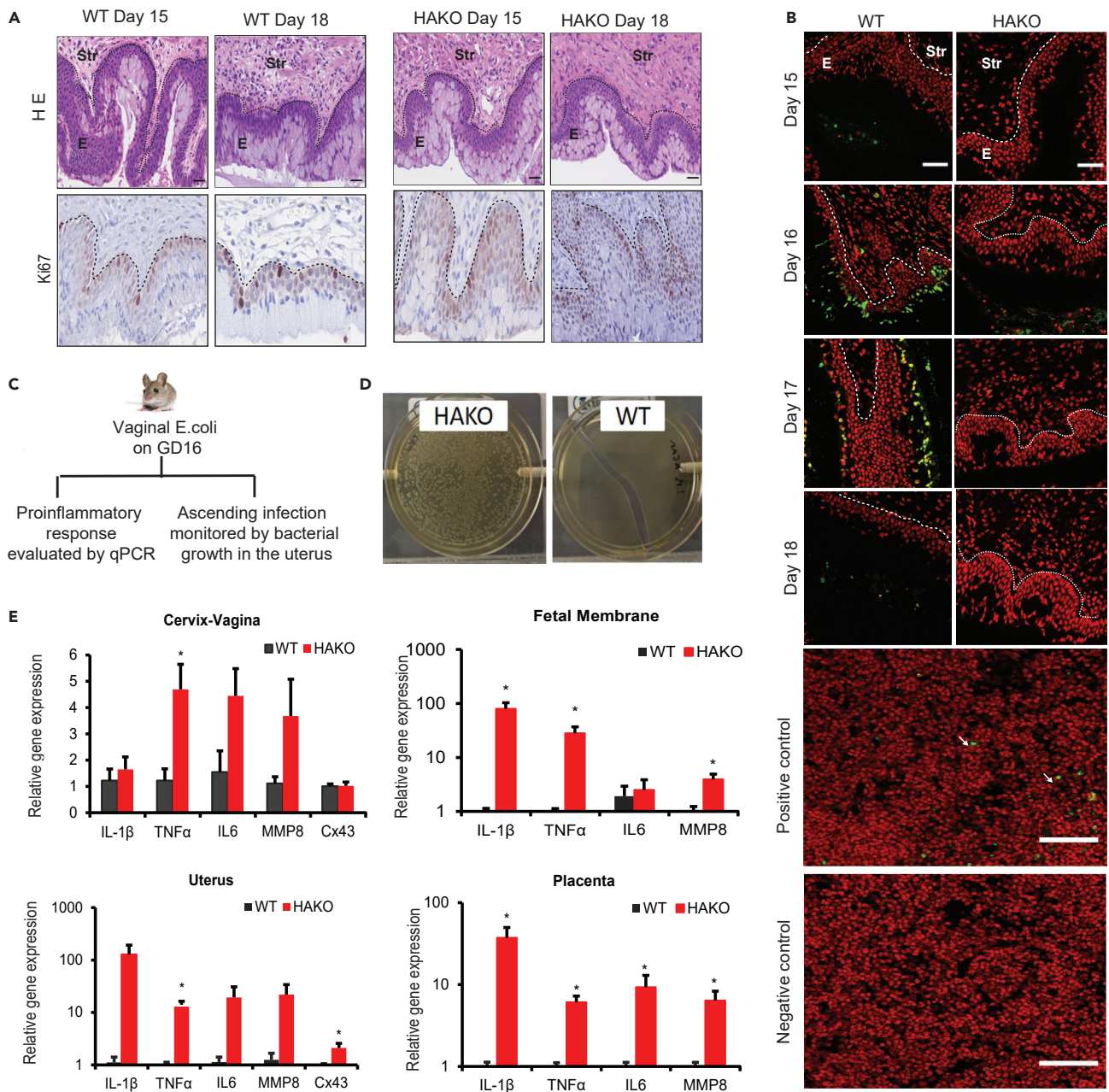


**Figure 6. Epithelial dysfunction in HAKO mice is associated with *E. coli* ascension and inflammation in maternal and fetal tissue**

(A) H&E staining (top), Ki67 (brown) immunostaining for proliferation (lower). H&E and Ki67 were done in WT and HAKO on GD15 and GD18. The representative images are shown at 60 $\times$  magnification from three independent samples per group. E: Epithelia; Str: Stroma. Scale bar 50  $\mu$ m.

(B) TUNEL imaging for cell death (red: nuclei, green:TUNEL<sup>+</sup>). TUNEL staining was done using WT and HAKO at GD15, 16, 17, and 18. Thymus from juvenile WT mice was used as positive (with terminal transferase) and negative (without transferase) control. The representative sections are shown at 20 $\times$  magnification. E: Epithelia; Str: Stroma Scale bar 50  $\mu$ m.

(C) Schematic of the vaginal *E. coli* inoculation and assessment for *E. coli* ascension and inflammation.

(D) Bacterial growth in uterine cultures from HAKO but not WT 24 h after the vaginal inoculation of *E. coli* demonstrates ascension of *E. coli* in HAKO.

(E) Quantitative real-time PCR analysis of proinflammatory genes (IL-1 $\beta$ , TNF- $\alpha$ , IL-6, and Mmp8) and a marker of uterine contractility (Cx43) expressed in tissues collected from WT (black) and HAKO (red). Expression was evaluated in cervix-vagina, uterus, fetal membrane, and placenta. N = 5 mice per genotype. Bar graphs depict the average relative gene expression  $\pm$  SEM Target gene expression was normalized to the housekeeping gene *Ppib* using the 2<sup>- $\Delta$</sup> -ddCt relative gene expression method (User Bulletin no.2; Applied Biosystems). \* indicates p < 0.05 (2-tailed ratio-paired Student's t test).

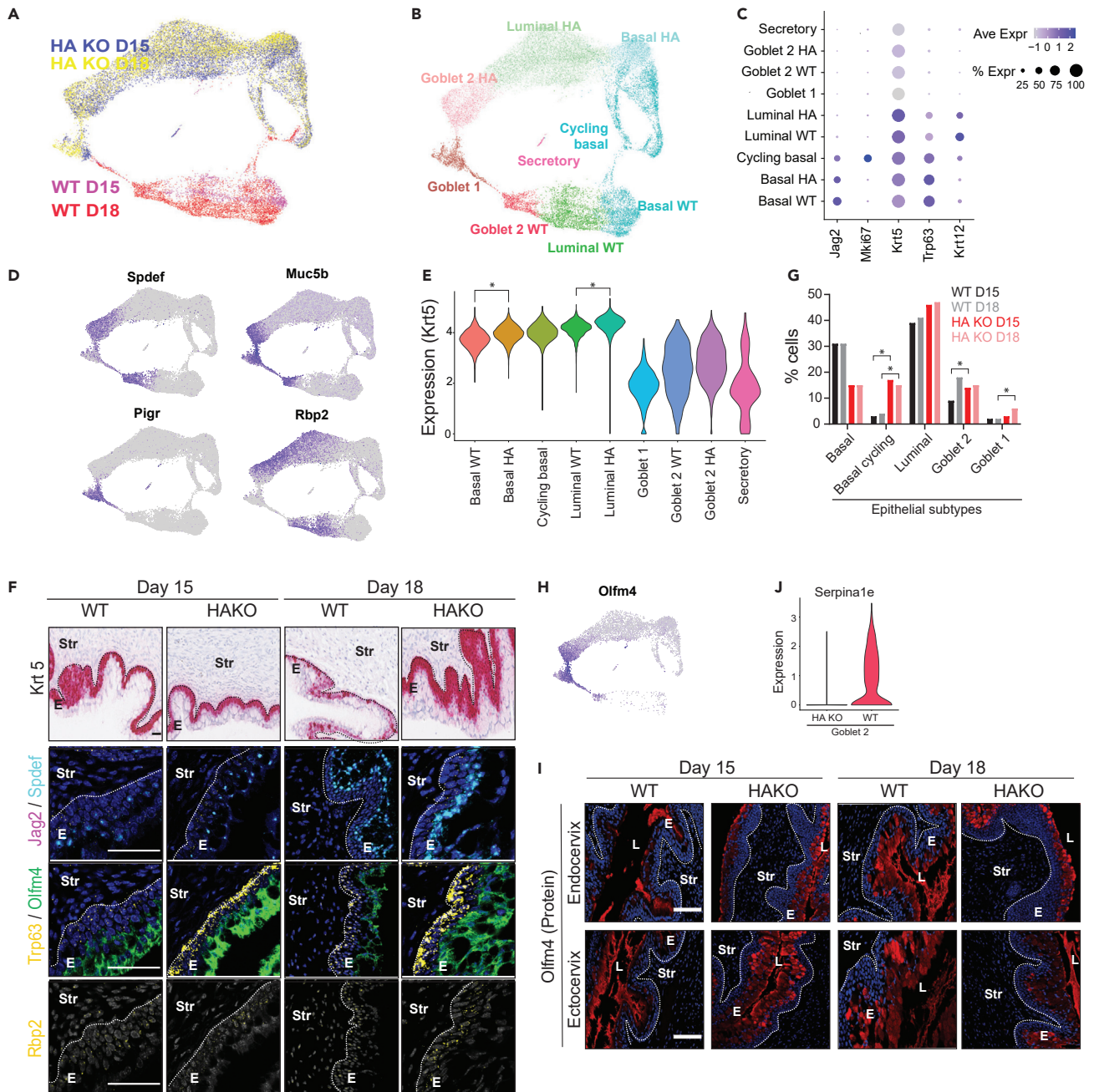


**Figure 7. Altered cell transition states characterize epithelial barrier disruption**

(A) UMAP visualization of WT and HAKO mice at GD15 and GD18. Cells are colored by genotype and time point.

(B) As in (A), but cells are colored by epithelial type.

(C) Dotplot showing the expression of basal and luminal markers in WT and HAKO cells. Cycling basal, Goblet 1 and secretory subtypes are not distinguished by genotype.

(D) Feature plots showing the expression of goblet markers.

(E) Violin plots for Krt5 expression. (\* indicates  $p < 0.01$ ).

(F) Comparison of the spatial and temporal pattern of epithelial cell markers in WT and HAKO at GD15 and GD18. Basal and luminal (Krt5, Jag2, and Trp63), or goblet (Spdef, Olfm4, and Rbp2) transcripts were analyzed by chromogenic or fluorescent RNAScope. Panel one: Krt5 (red). Panel two: Jag2 (pink) and Spdef (teal blue). Panel three: Trp63 (yellow) and Olfm4 (green). Panel four: Rbp2 (yellow). DAPI stains nuclei (blue or gray). E: Epithelia; Str: Stroma. Scale bar 50  $\mu$ m, objective lens 40 $\times$ . Representative images from three independent samples per each group.

(G) The abundance of epithelial subtypes in WT and HAKO mice at GD15-18. (Hypergeometric test  $p$  values:  $p_{\text{BasalCycling(D15 vs WT)}} = 9.48\text{E-}121$ ,  $p_{\text{Goblet Rbb2 (D15 vs WT)}} = 7.41\text{E-}18$ ,  $p_{\text{BasalCycling(D18 vs WT)}} = 5.83\text{E-}247$ ,  $p_{\text{Goblet pigr (D18 vs WT)}} = 9.63\text{E-}74$ , \* indicates  $p < 0.01$ ).

**Figure 7. Continued**

(H) Feature plot of Olfm4 expression.

(I) Olfm4 protein (red) expression in the HAKO cervical epithelia on GD15 and GD18 compared to wild type by IF staining. DAPI stains nuclei (blue). E: Epithelia; Str: Stroma. Scale bar 50  $\mu$ m, objective lens 20 $\times$ . Representative images from three independent samples per each group.

(J) Violin plot showing loss of Serpina1e expression in goblet 2 cluster in HAKO cells.

and luminal clusters relative to WT (Figure 7E) and this was confirmed in the GD18 HAKO endocervix by Krt5 spatial transcript analysis (Figure 7F). That loss of HA may disrupt basal cell transition cues is also suggested by the increased expression of Trp63, a transcription factor that drives differentiation of progenitor cells,<sup>43</sup> in GD15 and GD18 of HAKO relative to WT (Figures 7F and Figure S11A) and the significantly increased number of cycling basal cells relative to WT (Figure 7G). Immunofluorescent staining confirms increased Ki67 in the basal layer on GD15 and GD18 in HAKO relative to WT (Figure 6A). These patterns were noted in both the endocervix (Figure 6) and the ectocervix (data not shown).

In addition to the altered cell transition states in basal cells, Olfm4 expression was not confined to goblet 1 cells (Figure 7H). Strikingly, HAKO cells express Olfm4 at a low level in basal and non-secretory luminal cells and at a high level in goblet 1 and goblet 2 cells, while WT mice primarily express Olfm4 in goblet 1 cells. Consistent with the single-cell data, Rbp2<sup>+</sup> goblet 2 cells express Olfm4 transcripts in HAKO cervixes on GD15 and GD18 (Figure 7F), while cells co-expressing Rbp2 and Olfm4 are not visible in WT at either time point. In addition, transcripts for Olfm4 appear to increase in the GD15 and GD18 HAKO relative to WT. Olfm4 protein expression was assessed by IF staining (Figure 7I). Interestingly, the overall level of Olfm4 protein appeared similar between HAKO and WT on GD15 and GD18, yet Olfm4 was secreted into the cervical lumen in WT but remained primarily intracellular in the HAKO (Figures 7I and S11B). Secretion of Olfm4 has previously been demonstrated to downregulate inflammatory and immune responses in the gastrointestinal tract epithelia to limit damage to host tissue.<sup>53</sup> Goblet 2 cell dysfunction in HAKO mice was further supported by a dramatic loss of the Serpina1e (Figure 7J), a serine protease inhibitor that limits protease activity and inflammatory responses.<sup>62,63</sup> Serpina1e is the most significant hit ( $p_{WT\_vs\_KO} < 2.2e-16$ ). The total number of goblet cells appears similar between WT and HAKO as demonstrated by the Spdef expression (Figure 7F). Collectively, these results demonstrate hyaluronan regulates the balance between cell proliferation and subtype differentiation necessary for an immunoprotective barrier in pregnancy.

**DISCUSSION**

Epithelial dysfunction, which includes disruption of epithelial immune functions, is a key risk factor for preterm birth in both humans and mice. Mouse models are an important experimental system to better define the molecular and cellular regulation of epithelial-specific barriers and immune protection. A spatiotemporal profile of epithelial subtypes in the cervix of non-pregnant, pregnant, and laboring mice provides a necessary reference to define molecular and cellular regulation of the physical and immune barrier properties of the cervical epithelium. Through single-cell genomic analysis, we identified pregnancy-specific epithelial subtypes with distinct temporal abundance during cervical softening and ripening in the mouse endo- and ectocervix (Figure 8). Complementing the single-cell data, the spatial analysis identifies a similar expansion of these subtypes throughout the mouse endo- and ectocervix. Despite potential differences between human and mouse endocervical squamous and columnar epithelial composition, we identified striking similarities in the expression of mucins and secreted protective factors that collectively limit the ascension of pathogens and their contact with epithelial cells. These findings will improve understanding of epithelial functions necessary to maintain pregnancy as well as provide a reference to define dysregulation leading to cervical epithelial barrier disruption. This knowledge will improve understanding of host-pathogen interactions that support or compromise the function of the lower reproductive tract. Importantly, these findings will help uncover host response defects that contribute to the risk of ascending infection-mediated preterm birth.

Numerous advances arise from this work. Adding to the prior understanding that the cervical epithelium has a high turnover rate in the non-pregnant cycle and is highly proliferative in pregnancy,<sup>36</sup> we identify shifts in the pool of proliferating epithelial cells. On gestation day 6 and to a lesser extent day 12, both basal and luminal pools are proliferative yet in later gestation time points and IL basal cells are the dominant proliferative pool. The proliferative populations are present in both the endo- and ectocervix. Two proliferative luminal epithelial pools on GD6 were identified as luminal (Krt12<sup>+</sup>) and goblet (Spdef<sup>+</sup>) subtypes. The goblet subtype expresses markers of columnar epithelia (Krt8)<sup>64</sup> as well as Olfm4, a marker of intestinal stem/progenitor cells and a modulator of innate immunity.<sup>52,53,65</sup>

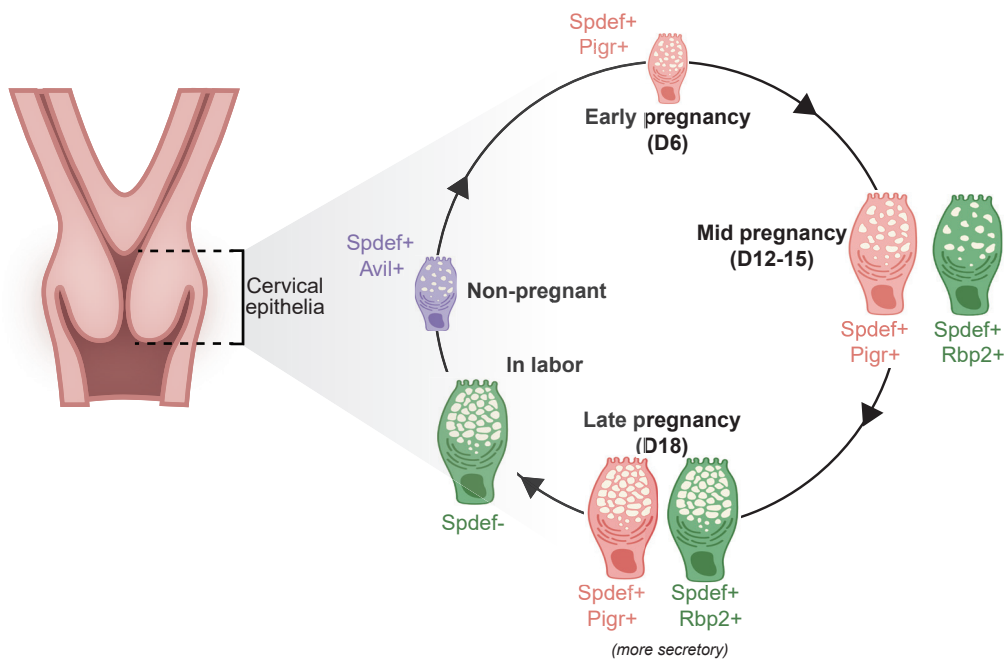


**Figure 8. Diverse goblet cell populations in mouse cervix during non-pregnant, pregnancy, and in labor**

Transcriptionally, non-pregnant goblet cells are distinct from the two goblet populations identified in pregnancy. Goblet cells in NP diestrus express the marker *Avil*. In early pregnancy (GD6), goblet cells are *Pigr*<sup>+</sup> and lack *Avil* expression. Two distinct goblet populations are identified on gestation days 12 and 15. One is *Pigr*<sup>+</sup> and the other is *Rbp2*<sup>+</sup>. On GD18, Goblet 2 population is more abundant than Goblet 1. Consistent with terminal differentiation of goblet cells in labor, transcriptional programs that drive goblet cell differentiation are lost and transcriptional programs in progenitor cells revert back to NP cell subtypes.

The marked shift in epithelial transcriptional programs and the pool of proliferating cells in early pregnancy resulted in distinct non-secretory and secretory luminal populations. For example, a single secretory goblet cell type was present on D6, while both non-goblet (*Ifitm1*<sup>+</sup>) and goblet (*Muc5b*<sup>+</sup>) secretory cells were identified in the NP secretory phase (diestrus). The goblet 1 population appears to be functionally distinct from the NP goblet. For example, goblet 1 cells express a sodium/calcium transporter (*Slc12a1*) and calcium channel regulator (*Clca1*) necessary to maintain ionic balance for mucus secretion<sup>66–68</sup> suggesting they may be more efficient in mucus secretion. In addition, fortification of goblet 1 epithelial immune defense is suggested by the increased expression of protease inhibitors belonging to the whey acidic protein family (*Slpi* and *Wfdc2*), polymeric Ig receptor (*Pigr*) necessary for the transport of IgA antibodies into the cervical lumen<sup>3</sup> and *Olfm4*, a secreted glycoprotein with a role in innate immunity.<sup>53,69</sup> Proteomic studies of cervical mucus from NP rhesus macaque<sup>70</sup> and proteomic or limited single-cell analysis of cervical samples from pregnant women highlight species conservation of noted factors observed in the goblet 1 cluster.<sup>12,71–74</sup>

Across the four gestational time points evaluated, two distinct goblet cell populations were identified, with a greater abundance of goblet 1 cells from GDs 6–15 while goblet 2 cells are greatest on GDs 15–18 (Figure 8). The noted decline in goblet 1 cells on GD18 is preceded by a spike in cell death of epithelial layers that line the lumen on GDs 16 and 17. Thus, the loss of goblet 1 cells is likely achieved by cell death. Not only do the two pregnancy-specific goblet populations have a distinct temporal pattern, RNA velocity analysis (Figure 4D) suggests goblet cluster 2 cells (but not goblet 1) arise from the differentiation of non-secretory luminal clusters. Further studies to determine lineage distinctions are warranted. From a functional standpoint, the two goblet populations appear similar but not identical. While both goblet 1 and goblet 2 cells express canonical goblet cell markers (*Spdef*, *Foxa3*, and *Agr2*),<sup>46,75</sup> the expression of numerous genes was lower in goblet 2 (e.g. *Muc1*, *Clca1*, *Cxcl15*, *Ltf*, and *Slpi*). In addition, goblet 2 cells express genes typically associated with luminal keratinocytes (*Sprr1a*, *Tgm5*, and *Sln*) similar to the NP secretory clusters. Recent studies describe the bactericidal role of the small proline-rich protein family members.<sup>76,77</sup> Thus, *Sprr1a* may provide antimicrobial protection in goblet 2 and NP secretory cells. Further studies to identify distinct functions of the heterogeneous population of pregnancy-distinct goblet cells in the mouse cervix are

warranted. Goblet cell functional heterogeneity has been described in intestinal crypts.<sup>78</sup> Collectively, these studies identify the expansion of two goblet subtypes in the mouse endo- and ectocervix that synthesize a distinct mucosal network, antimicrobials (e.g.  $\beta$ -defensin and *Sprr1*, and *Sprr2*), and protease inhibitors (e.g. *Sipi*, *Wfdc2*, *Wfdc15*, and *Wfdc18*). This customized arsenal of factors in pregnancy, we suggest, ensures epithelial homeostasis and provides innate immunity. In addition, the expression of immune cell chemoattractant cytokines such as *Cxcl1*, *Cxcl2*, and *Cxcl5* is low or absent in goblet clusters 1 and 2 in contrast to secretory cells in the NP cervix. The noted transcriptional changes would provide mucosal immunoprotection without eliciting proinflammatory responses that could induce preterm birth.

Goblet cell diversity with distinct antimicrobial molecule secretion and mucus gene expression may collectively contribute to ensuring barrier function during pregnancy. This process of inflammatory remodeling is potentially similar to that described in the barrier epithelium of the intestine and airways.<sup>79</sup> Importantly, the noted ability of the pregnancy-specific goblet subtypes to regulate the mucus structure, and display differential expression of chemokines/cytokines, antimicrobials, protease inhibitors, complement, and immunoglobulin transporters motivates further studies to define their regulation and function in the physiology of term pregnancy and spontaneous preterm birth (sPTB) in women. In further support, numerous studies highlight the association of sPTB in women with a diverse vaginal microbiota, reduced *Lactobacillus* content, and a maternal host immune response characterized by increases in proinflammatory cytokines, chemokines, antimicrobials, IgM/IgG, and complement activation.<sup>80–83</sup> In addition, reduced mucus permeability characterizes the cervical mucus of women who deliver preterm relative to term.<sup>22</sup>

The marked shift in the transcriptional program of epithelial cells during labor emphasizes the dynamic nature of epithelial cell homeostasis. Shortly after birth, mice transition to the estrus stage of the NP cycle (<sup>54–56</sup>). Our analysis of epithelial cells from NP, pregnant, and IL clearly demonstrates a marked change in the transcriptional program of epithelial cells during labor to initiate regeneration and differentiation of epithelial luminal subtypes present in the NP estrus cervix. In parallel, transcriptional programs necessary for goblet cell differentiation are downregulated. Despite this “behind the scenes” preparation during labor for the postpartum period, the differentiated goblet and non-goblet secretory cells that dominate the luminal epithelial layer ensure continued mucosal protection for the duration of parturition. The dynamic temporal change in epithelial subtypes from NP to pregnancy and the return to an NP pattern in labor is also reflected in the change in the expression of keratin intermediate filament proteins.<sup>44,84</sup>

In mice and women, the endocervix harbors columnar and squamous epithelial cells that are distinguished by expression of the keratin markers, *Krt 8* and *Krt 5*, respectively (<sup>24,25,26–31</sup>). Our data unexpectedly indicate the cervical secretory populations in NP and pregnancy express not only the columnar cell marker *Krt8* but also the squamous marker *Krt5*. These findings raise the possibility of cellular plasticity by which squamous cells transdifferentiate into the *Krt8*<sup>+</sup> secretory cells. Future lineage tracing studies will distinguish between a “physiological metaplasia” whereby squamous progenitor cells transform into secretory columnar cells or the alternative possibility that multiple progenitors give rise to diverse epithelial subtypes identified during pregnancy. The ability of a plastic bipotent cervical epithelial stem/progenitor cell to give rise to both squamous and columnar epithelia in humans and mice continues to be debated as demonstrated in recent studies which support<sup>85</sup> and refute<sup>64</sup> this hypothesis.

Future studies to define steroid hormone regulation of epithelial subtype diversity are needed. The role of progesterone and estrogen via activation of their nuclear receptors, progesterone receptor (Pgr), and estrogen receptor alpha and beta (ER $\alpha$ , ER $\beta$ ) in the regulation of NP cervical epithelial proliferation, differentiation, mucosal composition, and function is well documented.<sup>1,33,36,37,86,87</sup> Goblet cells are demonstrated to expand in the NP-proestrus cycle in mice with a *Muc5b*-GFP reporter thus indicating P4 and E2's ability to regulate specific epithelial subtypes.<sup>34</sup> Ongoing studies will leverage scATAC-Seq data to identify epithelial subtype-specific direct and indirect transcriptional targets of P4 and E2 through pregnancy and labor. However, one drawback is that the scATAC-Seq data presented here lack sufficient coverage of all epithelial subtypes sampled by scRNA-Seq, likely due to differences between the cellular isolation protocol of scRNA-Seq and nuclear isolation protocol of scATAC-Seq.

In women and mice, loss of secretory goblet cells or their dysfunction results in an increased risk of premature birth.<sup>14,23</sup> Additionally, the gel-forming mucin, *Muc5b*, made by goblet cells is reported to prevent the colonization of Group B *Streptococcus*, a pathogen associated with ascending infection.<sup>57</sup> Our studies in

mice lacking cervical hyaluronan (HAKO) indicate timely proliferation and differentiation of epithelial subpopulations is critical and in part regulated by hyaluronan. In the HAKO mice, elevated proliferation of basal cells with enhanced expression of Trp63, a transcription factor essential for the proliferative potential of stem/progenitor-stratified epithelia,<sup>88</sup> suggests HA prevents this expansion in normal pregnancy. Notably, goblet cell differentiation in the HAKO is relatively normal as they express canonical markers (eg: Spdef, Muc5b, Foxa3, and Agr2), though goblet cell organization and some aspects of function (e.g. loss of Serpina1e transcripts and reduced secretion of OLFM4 protein into the cervical lumen) are perturbed. While further interrogation of our data is required to define the hyaluronan signaling cues that are driving timely proliferation, differentiation, and organization of the mucosal epithelia, these findings highlight the necessity of finely regulated temporal changes in epithelial subtypes required for the maintenance of an optimal mucosal barrier through pregnancy.

The advent of single-cell technology has broadened our understanding of epithelial cell diversity necessary to maintain tissue homeostasis and the potential of host-microbe interactions to modify epithelial subtype populations or function in numerous tissues.<sup>89,90</sup> Our studies in the mouse cervix not only identify subtype heterogeneity but also suggest epithelial cell remodeling is necessary to maintain a dynamically shifting state of homeostasis in pregnancy and labor. The findings of the current study provide a framework to determine if perturbations in finely regulated signaling cues that drive epithelial proliferation, differentiation, and organization contribute to the risk of ascending infection. This research may lead to the identification of biomarkers that identify loss of cervical epithelial cell health in pregnancy and the development of preventive therapies that will reduce the risk of ascending inflammation-mediated preterm birth.

### Limitations of the study

There are several limitations to this study. This includes 1) the variation in the number of cervixes utilized for each time point to generate the single-cell libraries. This was necessitated by the reduced tissue weight/cell numbers of the NP and early pregnant cervix as compared to later time points in pregnancy and in labor. 2) The tissue digestion protocol was optimized for epithelial cell viability but was not optimal for the isolation of non-epithelial cell types such as fibroblasts, smooth muscle cells, endothelial cells, and immune cells. 3) The pooling of diestrus and estrus samples into a single library does not allow the assignment of cycle-specific epithelial subtypes though this was partially addressed by spatial analysis of RNA or protein. A recent study reports single-cell data for tissues throughout the female reproductive tract, including the cervix, at each stage of the estrus cycle in mice and will be a valuable comparison to our dataset (<https://www.biorxiv.org/content/10.1101/2022.10.26.513823v1>). 4) Though Pigr and Rbp2 clearly mark distinct clusters in the scRNA data, spatial analysis indicates most goblet cells (Spdef<sup>+</sup>) have overlapping Pigr and Rbp2 expression with very few cells expressing only Pigr or Rbp2 (Figures 4G and S5). This difference may be explained by limitations in the capture of all terminally differentiated goblet cells by scRNA-Seq.

### STAR★METHODS

Detailed methods are provided in the online version of this paper and include the following:

- **KEY RESOURCES TABLE**
- **RESOURCE AVAILABILITY**
  - Lead contact
  - Materials availability
  - Data and code availability
- **EXPERIMENTAL MODEL AND SUBJECT DETAILS**
  - Animals
  - Microbe strain
- **METHOD DETAILS**
  - Tissue collection
  - Single cervical cell dissociation and library preparation
  - Tissue fixation and histological evaluation
  - Immunohistochemistry
  - Immunofluorescence
  - *In situ* hybridization
  - Image analysis
  - Antibodies and probes

- Ascending infection by vaginal *E.coli* inoculation
- Single cell data clustering
- Single nuclei ATAC-Seq data analysis
- **QUANTIFICATION AND STATISTICAL ANALYSIS**

## SUPPLEMENTAL INFORMATION

Supplemental information can be found online at <https://doi.org/10.1016/j.isci.2023.105953>.

## ACKNOWLEDGMENTS

We acknowledge Jialei Duan for guidance with computational analysis. We acknowledge the BioHPC computational infrastructure at UT Southwestern for providing high-performance computing and storage resources that have contributed to the research results reported within this paper. We would like to acknowledge the assistance of the UT Southwestern Histo-Pathology Core and Quantitative Light Microscopy Core, a Shared Resource of the Harold C. Simmons Cancer Center, supported in part by an NCI Cancer Center Support Grant, 1P30 CA142543-01. We thank the UT Southwestern Medical Center Whole Brain Microscopy Facility (RRID: SCR\_017949) for assistance with whole slide imaging. This work is supported by the Burroughs Wellcome Fund (1019804) and 1P01HD087150-01A1 – Project 4 to M.M. G.C.H. is supported by CPRIT (RP190451), NIH (DP2GM128203, UM1HG011996), the Burroughs Wellcome Fund (1019804), and the Green Center for Reproductive Biological Sciences. M.C.C. is supported by the Ruth L. Kirschstein National Research Service Postdoctoral Fellowship (1F32 HD103314-01A1). A.C. and S.M. share equal co-authorship, and author order was determined by tossing a Hot Potato.

## AUTHOR CONTRIBUTIONS

M.M. and G.C.H. designed the experiments. L.W. performed the genomic experiments. A.C. performed computational analysis of genomic datasets, with assistance from E.S. S.P.M. performed single-cell isolation procedures, prepared sections and completed staining for RNA and protein studies and image analysis for H&E, TUNEL, IHC, IF, and RNAscope. M.C.C. performed nuclear isolation procedure for scATAC-Seq protocol. Y.A. performed the ascending infection experiment. All authors prepared the manuscript. M.M. and G.C.H. secured funding to support this project and provided intellectual support for all aspects of the work.

## DECLARATION OF INTERESTS

The authors declare no competing interests.

## INCLUSION AND DIVERSITY

We support inclusive, diverse, and equitable conduct of research.

Received: July 26, 2022

Revised: December 1, 2022

Accepted: January 5, 2023

Published: February 17, 2023

## REFERENCES

1. Wira, C.R., Rodriguez-Garcia, M., and Patel, M.V. (2015). The role of sex hormones in immune protection of the female reproductive tract. *Nat. Rev. Immunol.* *15*, 217–230.
2. Nallasamy, S., and Mahendroo, M. (2017). Distinct roles of cervical epithelia and stroma in pregnancy and parturition. *Semin. Reprod. Med.* *35*, 190–200.
3. Wira, C.R., Fahey, J.V., Sentman, C.L., Pioli, P.A., and Shen, L. (2005). Innate and adaptive immunity in female genital tract: cellular responses and interactions. *Immunol. Rev.* *206*, 306–335.
4. Sugiyama, M., Machida, N., Yasunaga, A., Terai, N., Fukasawa, H., Ono, H.K., Kobayashi, R., Nishiyama, K., Hashimoto, O., Kurusu, S., and Yoshioka, K. (2021). Vaginal mucus in mice: developmental and gene expression features of epithelial mucous cells during pregnancy. *Biol. Reprod.* *105*, 1272–1282.
5. Givan, A.L., White, H.D., Stern, J.E., Colby, E., Gosselin, E.J., Guyre, P.M., and Wira, C.R. (1997). Flow cytometric analysis of leukocytes in the human female reproductive tract: comparison of fallopian tube, uterus, cervix, and vagina. *Am. J. Reprod. Immunol.* *38*, 350–359.
6. Goode, D., Aravantinou, M., Jarl, S., Truong, R., Derby, N., Guerra-Perez, N., Kenney, J., Blanchard, J., Gettie, A., Robbiani, M., and Martinelli, E. (2014). Sex hormones selectively impact the endocervical mucosal microenvironment: implications for HIV transmission. *PLoS One* *9*, e97767.
7. Barrios De Tomasi, J., Opata, M.M., and Mowa, C.N. (2019). Immunity in the cervix: interphase between immune and cervical epithelial cells. *J. Immunol. Res.* *2019*, 7693183.
8. McShane, A., Bath, J., Jaramillo, A.M., Ridley, C., Walsh, A.A., Evans, C.M., Thornton, D.J.,

- and Ribbeck, K. (2021). *Curr. Biol.* 31, R938–R945.
9. Anahtar, M.N., Gootenberg, D.B., Mitchell, C.M., and Kwon, D.S. (2018). Cervicovaginal microbiota and reproductive health: the virtue of simplicity. *Cell Host Microbe* 23, 159–168.
  10. Hughes, B.L., Dutt, R., Raker, C., Barthelemy, M., Rossoll, R.M., Ramratnam, B., Wira, C.R., and Cu-Uvin, S. (2016). The impact of pregnancy on anti-HIV activity of cervicovaginal secretions. *Am. J. Obstet. Gynecol.* 215, 748.e1–748.e12.
  11. Anderson, B.L., Mendez-Figueroa, H., Dahlke, J.D., Raker, C., Hillier, S.L., and Cu-Uvin, S. (2013). Pregnancy-induced changes in immune protection of the genital tract: defining normal. *Am. J. Obstet. Gynecol.* 208, 321.e1–321.e9.
  12. Kutteh, W.H., and Franklin, R.D. (2001). Quantification of immunoglobulins and cytokines in human cervical mucus during each trimester of pregnancy. *Am. J. Obstet. Gynecol.* 184, 865–872.
  13. Walter, J., Fraga, L., Orin, M.J., Decker, W.D., Gipps, T., Stek, A., and Aldrovandi, G.M. (2011). Immunomodulatory factors in cervicovaginal secretions from pregnant and non-pregnant women: a cross-sectional study. *BMC Infect. Dis.* 11, 263.
  14. Ueda, Y., Mogami, H., Kawamura, Y., Takakura, M., Inohaya, A., Yasuda, E., Matsuzaka, Y., Chigusa, Y., Ito, S., Mandai, M., and Kondoh, E. (2022). Cervical MUC5B and MUC5AC are barriers to ascending pathogens during pregnancy. *J. Clin. Endocrinol. Metab.* 107, 3010–3021. <https://doi.org/10.1210/clinem/dgac545>.
  15. Becher, N., Adams Waldorf, K., Hein, M., and Ulbjerg, N. (2009). The cervical mucus plug: structured review of the literature. *Acta Obstet. Gynecol. Scand.* 88, 502–513.
  16. Burris, H.H., Riis, V.M., Schmidt, I., Gerson, K.D., Brown, A., and Elovitz, M.A. (2020). Maternal stress, low cervicovaginal  $\beta$ -defensin, and spontaneous preterm birth. *Am. J. Obstet. Gynecol. MFM* 2, 100092.
  17. Hezelgrave, N.L., Seed, P.T., Chin-Smith, E.C., Ridout, A.E., Shennan, A.H., and Tribe, R.M. (2020). Cervicovaginal natural antimicrobial expression in pregnancy and association with spontaneous preterm birth. *Sci. Rep.* 10, 12018.
  18. Smith-Dupont, K.B., Wagner, C.E., Witten, J., Conroy, K., Rudoltz, H., Pagidas, K., Snegovskikh, V., House, M., and Ribbeck, K. (2017). Probing the potential of mucus permeability to signify preterm birth risk. *Sci. Rep.* 7, 10302.
  19. Kyrgiou, M., Koliopoulos, G., Martin-Hirsch, P., Arbyn, M., Prendiville, W., and Paraskevidis, E. (2006). Obstetric outcomes after conservative treatment for intraepithelial or early invasive cervical lesions: systematic review and meta-analysis. *Lancet* 367, 489–498.
  20. Akgul, Y., Word, R.A., Ensign, L.M., Yamaguchi, Y., Lydon, J., Hanes, J., and Mahendroo, M. (2014). Hyaluronan in cervical epithelia protects against infection-mediated preterm birth. *J. Clin. Invest.* 124, 5481–5489.
  21. Pavlidis, I., Spiller, O.B., Sammut Demarco, G., MacPherson, H., Howie, S.E.M., Norman, J.E., and Stock, S.J. (2020). Cervical epithelial damage promotes *Ureaplasma parvum* ascending infection, intrauterine inflammation and preterm birth induction in mice. *Nat. Commun.* 11, 199.
  22. Critchfield, A.S., Yao, G., Jaishankar, A., Friedlander, R.S., Lieleg, O., Doyle, P.S., McKinley, G., House, M., and Ribbeck, K. (2013). Cervical mucus properties stratify risk for preterm birth. *PLoS One* 8, e69528.
  23. Lacroix, G., Gouyer, V., Rocher, M., Gottrand, F., and Desseyn, J.-L. (2022). A porous cervical mucus plug leads to preterm birth induced by experimental vaginal infection in mice. *iScience* 25, 104526.
  24. Singer, A. (1977). Dynamic anatomy of the cervical epithelium. *Adv. Exp. Med. Biol.* 89, 77–89.
  25. Cunha, G.R., Kurita, T., Cao, M., Shen, J., Robboy, S., and Baskin, L. (2017). Molecular mechanisms of development of the human fetal female reproductive tract. *Differentiation.* 97, 54–72.
  26. Cunha, G.R., Sinclair, A., Ricke, W.A., Robboy, S.J., Cao, M., and Baskin, L.S. (2019). *Reproductive tract biology: of mice and men.* *Differentiation.* 110, 49–63.
  27. Fishbeck, D.W., and Sebastiani, A. (2015). *Comparative Anatomy: Manual of Vertebrate Dissection* (Morton Publishing Company).
  28. Leppi, T.J., and John Leppi, T. (1964). A study of the uterine cervix of the mouse. *Anat. Rec.* 150, 51–65. <https://doi.org/10.1002/ar.1091500106>.
  29. Mehta, F.F., Son, J., Hewitt, S.C., Jang, E., Lydon, J.P., Korach, K.S., and Chung, S.-H. (2016). Distinct functions and regulation of epithelial progesterone receptor in the mouse cervix, vagina, and uterus. *Oncotarget* 7, 17455–17467.
  30. P.M. Treuting, S.M. Dintzis, D. Liggitt, and C.W. Frevert, eds. (2011). *Comparative anatomy and histology: A mouse and human atlas (expert consult)* (Academic Press).
  31. Graham, C.E. (1966). Cyclic changes in the squamo-columnar junction of the mouse cervix uteri. *Anat. Rec.* 155, 251–260.
  32. Kurita, T., Cooke, P.S., and Cunha, G.R. (2001). Epithelial-stromal tissue interaction in paramesonephric (Müllerian) epithelial differentiation. *Dev. Biol.* 240, 194–211.
  33. Gipson, I.K., Ho, S.B., Spurr-Michaud, S.J., Tisdale, A.S., Zhan, Q., Torlakovic, E., Pudney, J., Anderson, D.J., Toribara, N.W., and Hill, J.A., 3rd (1997). Mucin genes expressed by human female reproductive tract epithelia. *Biol. Reprod.* 56, 999–1011.
  34. Portal, C., Gouyer, V., Magnien, M., Plet, S., Gottrand, F., and Desseyn, J.-L. (2017). In vivo imaging of the Muc5b gel-forming mucin. *Sci. Rep.* 7, 44591.
  35. Richardson, J., Kaushic, C., and Wira, C.R. (1993). Estradiol regulation of secretory component: expression by rat uterine epithelial cells. *J. Steroid Biochem. Mol. Biol.* 47, 143–149.
  36. Ramos, J.G., Varayoud, J., Bosquiaz, V.L., Luque, E.H., and Muñoz-de-Toro, M. (2002). Cellular turnover in the rat uterine cervix and its relationship to estrogen and progesterone receptor dynamics. *Biol. Reprod.* 67, 735–742.
  37. Galand, P., Leroy, F., and Chrétien, J. (1971). Effect of oestradiol on cell proliferation and histological changes in the uterus and vagina of mice. *J. Endocrinol.* 49, 243–252.
  38. Read, C.P., Word, R.A., Ruschinsky, M.A., Timmons, B.C., and Mahendroo, M.S. (2007). Cervical remodeling during pregnancy and parturition: molecular characterization of the softening phase in mice. *Reproduction* 134, 327–340.
  39. Garcia-Flores, V., Romero, R., Peyvandipour, A., Galaz, J., Pusod, E., Panaitescu, B., Miller, D., Xu, Y., Tao, L., Liu, Y., et al. (2022). The single-cell atlas of the murine reproductive tissues during preterm labor. Preprint at bioRxiv. <https://doi.org/10.1101/2022.04.27.489704>.
  40. Becht, E., McInnes, L., Healy, J., Dutertre, C.-A., Kwok, I.W.H., Ng, L.G., Ginhoux, F., and Newell, E.W. (2018). Dimensionality reduction for visualizing single-cell data using UMAP. *Nat. Biotechnol.* 37, 38–44. <https://doi.org/10.1038/nbt.4314>.
  41. Satpathy, A.T., Granja, J.M., Yost, K.E., Qi, Y., Meschi, F., McDermott, G.P., Olsen, B.N., Mumbach, M.R., Pierce, S.E., Corces, M.R., et al. (2019). Massively parallel single-cell chromatin landscapes of human immune cell development and intratumoral T cell exhaustion. *Nat. Biotechnol.* 37, 925–936.
  42. Granja, J.M., Corces, M.R., Pierce, S.E., Bagdatli, S.T., Choudhry, H., Chang, H.Y., and Greenleaf, W.J. (2021). ArchR is a scalable software package for integrative single-cell chromatin accessibility analysis. *Nat. Genet.* 53, 403–411.
  43. Koster, M.I., Kim, S., Mills, A.A., DeMayo, F.J., and Roop, D.R. (2004). p63 is the molecular switch for initiation of an epithelial stratification program. *Genes Dev.* 18, 126–131.
  44. Karantz, V. (2011). Keratins in health and cancer: more than mere epithelial cell markers. *Oncogene* 30, 127–138.
  45. Kasetti, R.B., Gaddipati, S., Tian, S., Xue, L., Kao, W.W.-Y., Lu, Q., and Li, Q. (2016). Study of corneal epithelial progenitor origin and the Yap1 requirement using keratin 12 lineage tracing transgenic mice. *Sci. Rep.* 6, 35202.
  46. Chen, G., Korfhagen, T.R., Xu, Y., Kitzmiller, J., Wert, S.E., Maeda, Y., Gregorieff, A., Clevers, H., and Whitsett, J.A. (2009). SPDEF is required for mouse pulmonary goblet cell

- differentiation and regulates a network of genes associated with mucus production. *J. Clin. Invest.* 119, 2914–2924.
47. Knoop, K.A., and Newberry, R.D. (2018). Goblet cells: multifaceted players in immunity at mucosal surfaces. *Mucosal Immunol.* 11, 1551–1557.
  48. Schmitz, J.M., McCracken, V.J., Dimmitt, R.A., and Lorenz, R.G. (2007). Expression of CXCL15 (Lungkine) in murine gastrointestinal, urogenital, and endocrine organs. *J. Histochem. Cytochem.* 55, 515–524.
  49. Wang, P., Wu, S.-P., Brooks, K.E., Kelleher, A.M., Milano-Foster, J.J., DeMayo, F.J., and Spencer, T.E. (2018). Generation of mouse for conditional expression of forkhead box A2. *Endocrinology* 159, 1897–1909.
  50. Kim, T.H., and Jeong, J.-W. (2019). Proline-rich acidic protein 1 (PRAP1) is a target of ARID1A and PGR in the murine uterus. *Dev. Reprod.* 23, 277–284.
  51. Li, H., Chaitankar, V., Zhu, J., Chin, K., Liu, W., Pirooznia, M., and Rodgers, G.P. (2020). Olfactomedin 4 mediates stem/progenitor-like cell proliferation and differentiation via MYC. *Sci. Rep.* 10, 21924.
  52. Schuijers, J., van der Flier, L.G., van Es, J., and Clevers, H. (2014). Robust cre-mediated recombination in small intestinal stem cells utilizing the *olm4* locus. *Stem Cell Rep.* 3, 234–241.
  53. Liu, W., Yan, M., Liu, Y., Wang, R., Li, C., Deng, C., Singh, A., Coleman, W.G., Jr., and Rodgers, G.P. (2010). Olfactomedin 4 down-regulates innate immunity against *Helicobacter pylori* infection. *Proc. Natl. Acad. Sci. USA.* 107, 11056–11061.
  54. Connor, J.R., and Davis, H.R. (1980). Postpartum estrus in Norway rats. I. Behavior. *Biol. Reprod.* 23, 994–999.
  55. Morrison, P., Dieterich, R., and Preston, D. (1976). Breeding and reproduction of fifteen wild rodents maintained as laboratory colonies. *Lab. Anim. Sci.* 26, 237–243.
  56. Gilbert, A.N. (1984). Postpartum and lactational estrus: a comparative analysis in rodentia. *J. Comp. Psychol.* 98, 232–245.
  57. Burcham, L.R., Bath, J.R., Werlang, C.A., Lyon, L.M., Liu, N., Evans, C., Ribbeck, K., and Doran, K.S. (2022). Role of MUC5B during group B streptococcal vaginal colonization. *mBio* 13, e0003922.
  58. Lacroix, G., Gouyer, V., Gottrand, F., and Desseyn, J.-L. (2020). The cervicovaginal mucus barrier. *Int. J. Mol. Sci.* 21, 8266. <https://doi.org/10.3390/ijms21218266>.
  59. Vornhagen, J., Quach, P., Boldenow, E., Merillat, S., Whidbey, C., Ngo, L.Y., Adams Waldorf, K.M., and Rajagopal, L. (2016). Bacterial hyaluronidase promotes ascending GBS infection and preterm birth. *mBio* 7, e00781–e00816. <https://doi.org/10.1128/mBio.00781-16>.
  60. Mahendroo, M. (2019). Cervical hyaluronan biology in pregnancy, parturition and preterm birth. *Matrix Biol.* 78–79, 24–31.
  61. Straach, K.J., Shelton, J.M., Richardson, J.A., Hascall, V.C., and Mahendroo, M.S. (2005). Regulation of hyaluronan expression during cervical ripening. *Glycobiology* 15, 55–65.
  62. Borel, F., Sun, H., Zieger, M., Cox, A., Cardozo, B., Li, W., Oliveira, G., Davis, A., Gruntman, A., Flotte, T.R., et al. (2018). Editing out five paralogs to create a mouse model of genetic emphysema. *Proc. Natl. Acad. Sci. USA.* 115, 2788–2793.
  63. Lomas, D.A., and Silverman, E.K. (2001). The genetics of chronic obstructive pulmonary disease. *Respir. Res.* 2, 20–26.
  64. Chumduri, C., Gurumurthy, R.K., Berger, H., Dietrich, O., Kumar, N., Koster, S., Brinkmann, V., Hoffmann, K., Drabkina, M., Arampatz, P., et al. (2021). Opposing Wnt signals regulate cervical squamocolumnar homeostasis and emergence of metaplasia. *Nat. Cell Biol.* 23, 184–197.
  65. Itzkovitz, S., Lyubimova, A., Blat, I.C., Maynard, M., van Es, J., Lees, J., Jacks, T., Clevers, H., and van Oudenaarden, A. (2011). Single-molecule transcript counting of stem-cell markers in the mouse intestine. *Nat. Cell Biol.* 14, 106–114.
  66. Gagnon, K.B., and Delpire, E. (2013). Physiology of SLC12 transporters: lessons from inherited human genetic mutations and genetically engineered mouse knockouts. *Am. J. Physiol. Cell Physiol.* 304, C693–C714.
  67. Erickson, N.A., Mundhenk, L., Giovannini, S., Glaubien, R., Heimesaat, M.M., and Gruber, A.D. (2016). Role of goblet cell protein CLCA1 in murine DSS colitis. *J. Inflamm.* 13, 5.
  68. Liu, C.-L., and Shi, G.-P. (2019). Calcium-activated chloride channel regulator 1 (CLCA1): more than a regulator of chloride transport and mucus production. *World Allergy Organ. J.* 12, 100077.
  69. Liu, W., Yan, M., Sugui, J.A., Li, H., Xu, C., Joo, J., Kwon-Chung, K.J., Coleman, W.G., and Rodgers, G.P. (2013). *Olfm4* deletion enhances defense against *Staphylococcus aureus* in chronic granulomatous disease. *J. Clin. Invest.* 123, 3751–3755.
  70. Han, L., Park, D., Reddy, A., Wilmarth, P.A., and Jensen, J.T. (2021). Comparing endocervical mucus proteome of humans and rhesus macaques. *Proteomics. Clin. Appl.* 15, e2100023.
  71. Barnum, C.E., Shetye, S.S., Fazelinia, H., Garcia, B.A., Fang, S., Alzamora, M., Li, H., Brown, L.M., Tang, C., Myers, K., et al. (2022). The non-pregnant and pregnant human cervix: a systematic proteomic analysis. *Reprod. Sci.* 29, 1542–1559. <https://doi.org/10.1007/s43032-022-00892-4>.
  72. Lee, D.-C., Hassan, S.S., Romero, R., Tarca, A.L., Bhatti, G., Gervasi, M.T., Caruso, J.A., Stemmer, P.M., Kim, C.J., Hansen, L.K., et al. (2011). Protein profiling underscores immunological functions of uterine cervical mucus plug in human pregnancy. *J. Proteomics* 74, 817–828.
  73. Koh, W., Wu, A., Penland, L., Treutlein, B., Neff, N.F., Mantalas, G.L., Blumenfeld, Y.J., El-Sayed, Y.Y., Stevenson, D.K., Shaw, G.M., and Quake, S.R. (2019). Single cell transcriptomes derived from human cervical and uterine tissue during pregnancy. *Adv. Biosyst.* 3, e1800336.
  74. Orfanelli, T., Jayaram, A., Doulaveris, G., Forney, L.J., Ledger, W.J., and Witkin, S.S. (2014). Human epididymis protein 4 and secretory leukocyte protease inhibitor in vaginal fluid: relation to vaginal components and bacterial composition. *Reprod. Sci.* 21, 538–542.
  75. Rajavelu, P., Chen, G., Xu, Y., Kitzmiller, J.A., Korfhagen, T.R., and Whitsett, J.A. (2015). Airway epithelial SPDEF integrates goblet cell differentiation and pulmonary Th2 inflammation. *J. Clin. Invest.* 125, 2021–2031.
  76. Hu, Z., Zhang, C., Sifuentes-Dominguez, L., Zarek, C.M., Propheter, D.C., Kuang, Z., Wang, Y., Pendse, M., Ruhn, K.A., Hassell, B., et al. (2021). Small proline-rich protein 2A is a gut bactericidal protein deployed during helminth infection. *Science* 374, eabe6723.
  77. Zhang, C., Hu, Z., Lone, A.G., Artami, M., Edwards, M., Zouboulis, C.C., Stein, M., and Harris-Tryon, T.A. (2022). Small proline-rich proteins (SPRRs) are epidermally produced antimicrobial proteins that defend the cutaneous barrier by direct bacterial membrane disruption. *Elife* 11, e76729. <https://doi.org/10.7554/eLife.76729>.
  78. Nyström, E.E.L., Martínez-Abad, B., Arike, L., Birchenough, G.M.H., Nonnecke, E.B., Castillo, P.A., Svensson, F., Bevins, C.L., Hansson, G.C., and Johansson, M.E.V. (2021). An intercrypt subpopulation of goblet cells is essential for colonic mucus barrier function. *Science* 372, eabb1590. <https://doi.org/10.1126/science.abb1590>.
  79. Medzhitov, R. (2021). The spectrum of inflammatory responses. *Science* 374, 1070–1075.
  80. Chan, D., Bennett, P.R., Lee, Y.S., Kundu, S., Teoh, T.G., Adan, M., Ahmed, S., Brown, R.G., David, A.L., Lewis, H.V., et al. (2022). Microbial-driven preterm labour involves crosstalk between the innate and adaptive immune response. *Nat. Commun.* 13, 975.
  81. Elovitz, M.A., Gajer, P., Riis, V., Brown, A.G., Humphrys, M.S., Holm, J.B., and Ravel, J. (2019). Cervicovaginal microbiota and local immune response modulate the risk of spontaneous preterm delivery. *Nat. Commun.* 10, 1305.
  82. Florova, V., Romero, R., Tarca, A.L., Galaz, J., Motomura, K., Ahmad, M.M., Hsu, C.-D., Hsu, R., Tong, A., Ravel, J., et al. (2021). Vaginal host immune-microbiome interactions in a cohort of primarily African-American women who ultimately underwent spontaneous preterm birth or delivered at term. *Cytokine* 137, 155316.
  83. Flaviani, F., Hezelgrave, N.L., Kanno, T., Prosdoci, E.M., Chin-Smith, E., Ridout,

- A.E., von Maydell, D.K., Mistry, V., Wade, W.G., Shennan, A.H., et al. (2021). Cervicovaginal microbiota and metabolome predict preterm birth risk in an ethnically diverse cohort. *JCI Insight* 6, e149257. <https://doi.org/10.1172/jci.insight.149257>.
84. Harmon, R.M., Simpson, C.L., Johnson, J.L., Koetsier, J.L., Dubash, A.D., Najor, N.A., Sarig, O., Sprecher, E., and Green, K.J. (2013). Desmoglein-1/Erbin interaction suppresses ERK activation to support epidermal differentiation. *J. Clin. Invest.* 123, 1556–1570.
85. Zhao, Z., Wang, Y., Wu, Y., Li, D., Zhang, T., Ma, Y., Teng, X., and Zuo, W. (2021). Single-cell analysis defines the lineage plasticity of stem cells in cervix epithelium. *Cell Regen.* 10, 36.
86. Ludwig, K. (1989). [Homogeneity and corrosion resistance of cast dental precious metal alloys compared with uncast alloys]. *Dtsch. Zahnärztl. Z.* 44, 905–907.
87. Wang, H., Stjernholm, Y., Ekman, G., Eriksson, H., and Sahlin, L. (2001). Different regulation of oestrogen receptors alpha and beta in the human cervix at term pregnancy. *Mol. Hum. Reprod.* 7, 293–300.
88. Senoo, M., Pinto, F., Crum, C.P., and McKeon, F. (2007). p63 Is essential for the proliferative potential of stem cells in stratified epithelia. *Cell* 129, 523–536.
89. Bomidi, C., Robertson, M., Coarfa, C., Estes, M.K., and Blutt, S.E. (2021). Single-cell sequencing of rotavirus-infected intestinal epithelium reveals cell-type specific epithelial repair and tuft cell infection. *Proc. Natl. Acad. Sci. USA.* 118, e2112814118. <https://doi.org/10.1073/pnas.2112814118>.
90. Parikh, K., Antanaviciute, A., Fawcner-Corbett, D., Jagielowicz, M., Aulicino, A., Lagerholm, C., Davis, S., Kinchen, J., Chen, H.H., Alham, N.K., et al. (2019). Colonic epithelial cell diversity in health and inflammatory bowel disease. *Nature* 567, 49–55.
91. Byers, S.L., Wiles, M.V., Dunn, S.L., and Taft, R.A. (2012). Mouse estrous cycle identification tool and images. *PLoS One* 7, e35538.
92. Stuart, T., Butler, A., Hoffman, P., Hafemeister, C., Papalexi, E., Mauck, W.M., 3rd, Hao, Y., Stoeckius, M., Smibert, P., and Satija, R. (2019). Comprehensive integration of single-cell data. *Cell* 177, 1888–1902.e21.

STAR★METHODS

KEY RESOURCES TABLE

REAGENT or RESOURCE	SOURCE	IDENTIFIER
<b>Antibodies</b>		
Rabbit anti-Keratin 10	Abcam	ab76318; RRID:AB_1523465
mouse anti-IFITM1	Proteintech	60074-1; RRID:AB_2233405
Rat anti-ki67	ThermoFisher scientific	14-5698-82
chicken anti-Keratin 5	Biolegend	905901; RRID:AB_2565054
Rabbit anti-Keratin 8	Abcam	ab53280; RRID:AB_869901
Biotinylated goat anti-rabbit IgG	Vector laboratories	BA-1000; RRID:AB_2313606
Biotinylated goat anti-mouse IgG	Vector laboratories	BA-9200; RRID:AB_2336171
Biotinylated goat anti-Rat IgG	Vector laboratories	BA-9400; RRID:AB_2336202
Donkey anti-chicken Alexa Fluor 488	Jackson ImmunoResearch	703-545-155; RRID:AB_2340375
Goat anti-rabbit Alexa Fluor 594	Thermo Fisher	A-11012; RRID:AB_2534079
<b>Bacterial and virus strains</b>		
<i>E. coli</i> (strain : CDC 5624-50 [NCTC 9701])	ATCC	12014
<b>Chemicals, peptides, and recombinant proteins</b>		
Chromogenic Kit	Advanced cell diagnostics	320511
Multiplex fluorescent	Advanced cell diagnostics	323100
Krt5 probe	Advanced cell diagnostics	415041
Avil probe	Advanced cell diagnostics	498531
Dsg1a probe	Advanced cell diagnostics	842861
Spdef probe	Advanced cell diagnostics	544421
Muc5b probe	Advanced cell diagnostics	471991
Muc1 probe	Advanced cell diagnostics	421871
Pigr probe	Advanced cell diagnostics	552591
Rbp2 probe	Advanced cell diagnostics	444091
Olfm4 probe	Advanced cell diagnostics	311831
<b>Critical commercial assays</b>		
Chromium Next GEM Single Cell 3' GEM, Library & Gel Bead Kit v3.1	10X Genomics	1000121
Chromium Next GEM Single Cell ATAC Library & Gel Bead Kit v1.1	10X Genomics	1000175
<b>Deposited data</b>		
Sequencing data from this study	Gene Expression Omnibus	GEO: GSE196529
<b>Experimental models: Organisms/strains</b>		
Has1 -/-	Kobayashi N, et al., 2010	N/A
Has3 -/-	Bai K-J, et al, 2005	N/A
Has 2 fl/fl	Matsumoto K, et al., 2009	N/A
PR-Cre	Soyal SM, et al., 2005	N/A
C57BL6/129 Mouse strain		Taconic B6129F1   Taconic Biosciences

(Continued on next page)

**Continued**

REAGENT or RESOURCE	SOURCE	IDENTIFIER
<b>Oligonucleotides</b>		
Mouse IL-1B Forward: 5'- GCC CAT CCT CTG TGA CTC ATG-3' Reverse: 5' - AGC CTG TAG TGC AGC TGT CTA ATG-3'	This paper	
MouseTNF-ALPHA Forward: 5'- CTG AGG TCA ATC TGC CCA AGT AC-3' Reverse: 5'- CTT CAC AGA GCA ATG ACT CCA AAG-3'	This paper	
Mouse IL-6 Forward: 5'- TCG TGG AAA TGA GAA AAG AGT TG -3' Reverse: 5'- AGT GCA TCA TCG TTG TTC ATA CA-3'	This paper	
Mouse MMP-8 Forward: 5'- GATTCAGAAGAAACGTGGAC TCAA -3' Reverse: 5- CATCAAGGCACCCAGGAT CAGT-3'	This paper	
Mouse CX43 Forward: 5'- TGG ACA AGG TCC AAG CCT ACT C -3' Reverse: 5'- TCC CCA GGA GCA GGA TTC T-3'	This paper	
Mouse Cyclophilin Forward: 5'- TGGAGAGCACCAAGACA GACA-3' Reverse: 5- TGCCGGAGTCGACAATGAT-3'	This paper	
<b>Software and algorithms</b>		
Fiji/Image J	U.S National Institutes of Health	Download ( <a href="https://imagej.nih.gov/ij/">nih.gov</a> ) <a href="https://imagej.nih.gov/ij/">https://imagej.nih.gov/ij/</a> RRID:SCR_003070
NDP.View2	HAMAMATSU	NDP.view2 Viewing software U12388-01   Hamamatsu Photonics
ZEN 3.0	Zeiss	RRID:SCR_013672
Code for single-cell RNA-Seq analysis	This paper	GitHub.com/ <a href="https://github.com/ancooley/Cervix_scRNA-seq">ancooley/Cervix_scRNA-seq</a>

**RESOURCE AVAILABILITY**

**Lead contact**

Information and requests for resources and reagents should be directed to and will be fulfilled by the lead contact, Mala Mahendroo ([mala.mahendroo@utsouthwestern.edu](mailto:mala.mahendroo@utsouthwestern.edu)).

**Materials availability**

This study did not generate new unique reagents.

**Data and code availability**

- Single-cell RNA-seq data have been deposited at GEO and are publicly available as of the date of publication. Accession numbers are listed in the [key resources table](#). All original code has been deposited at GitHub and is publicly available as of the date of publication. DOIs are listed in the [key resources table](#). Microscopy data reported in this paper will be shared by the [lead contact](#) upon request.

- Any additional information required to reanalyze the data reported in this paper is available from the [lead contact](#) upon request.

## EXPERIMENTAL MODEL AND SUBJECT DETAILS

### Animals

All experimental procedures with mice were approved by the Institutional Animal Care and Use Committee at the University of Texas Southwestern Medical Center. Mice were housed under a 12-hour light/dark cycle at 22°C in a barrier facility and were provided with food and water *ad libitum*. Mice used in this study were 2- to 6-month-old nulliparous females. **Non-pregnant** mice were assessed for the stage of the estrus cycle. To determine the cycle, vaginal smears were taken and analyzed for the presence or absence of cornified epithelia, nucleated epithelia and leukocytes.<sup>91</sup> To generate timed **pregnant and in labor mice**, females were housed with males from 9am to 2pm at which time females were evaluated for the presence of a vaginal plug. The day of plug formation was counted as day 0 with birth occurring on gestation day 19. In labor (IL) samples were collected on d19 after visual monitoring for the delivery of 1-2 pups. Mice used in this study were of C57B6/129SV strain. As previously described, the Has1/2/3 knockout mouse line has global loss of hyaluronan synthase 1 and 3 (Has1<sup>-/-</sup> and Has3<sup>-/-</sup>) and cell-specific loss of Has2 in cells expressing progesterone receptor (Has2<sup>fl/fl</sup>; PRCre<sup>+/-</sup>).<sup>20</sup> Mice used in this study are Has1<sup>-/-</sup>, Has3<sup>-/-</sup>, Has2<sup>fl/fl</sup> PRCre<sup>+/-</sup>. These mice are referred to as HAKO in this study.

### Microbe strain

*Escherichia coli* strain CDC 5624-50 [NCTC 9701] was used to elicit infection-induced preterm birth in mice. *Escherichia coli* serotype O55 was grown aerobically with shaking at 37°C in Luria-Bertani medium. *Escherichia coli* were grown to the mid-logarithmic phase and colony forming units (CFU) were estimated by measuring the optical density at 600 nm (OD 600).

## METHOD DETAILS

### Tissue collection

For the single cell studies cervixes were collected by dissection below the transition zone (TZ) (Figure 1) and all vaginal tissue was removed. For spatial studies, cervixes with vagina and uterine horns were collected for longitudinal sections with the cervical canal evident throughout each section and in the same longitudinal plane as the uterine horns.

### Single cervical cell dissociation and library preparation

Cells for the single-cell RNA libraries, were isolated from cervixes of NP (diestrus (n = 7) and estrus (n = 2)) and gestational days 6 (n = 5), 12 (n = 4), 15 (n = 3), 18 (n = 3), and IL (n = 3). The number of pooled cervixes used for each library is indicated. Tissues were minced with a sterile razor. Minced cervixes were dissociated with 10 mg/ml cold protease (Sigma-Aldrich) with 1 mg/ml DNase I (Roche) and 0.5 M EDTA (Fisher Scientific). After a 60 min incubation at 4°C, cells were filtered through a 40 µm cell strainer (BD Biosciences) and washed twice with fresh ice cold 1x PBS and then resuspended in 1x PBS +0.005% BSA. Cell viability and numbers were assessed by trypan blue stain and counted using Hemocytometer. scRNA-Seq was carried out as recommended by the 10X Genomics standard operating procedure.

Nuclei for the single cell ATAC-Seq (scATAC-Seq) libraries were isolated from frozen mouse cervixes of NP metestrus (n = 2) and gestational days 6 (n = 3), 12 (n = 2), 15 (n = 2), 18 (n = 1) and IL (n = 1) following 10X Genomics protocol. Briefly, cervixes were homogenized in 0.1X Lysis buffer with a pellet pestle for 5 minutes on ice. The reaction was stopped by adding the wash buffer to the lysed cells and suspensions were filtered through a 40µm cell strainer (BD Biosciences). Nuclei concentration was determined by DAPI and Ethidium Homodimer-1 dyes using a Countess II FL Automated Cell Counter. scATAC-Seq was conducted as recommended by the 10X Genomics User Guide.

### Tissue fixation and histological evaluation

All tissues were fixed in 4% paraformaldehyde (Sigma-Aldrich) in 1x PBS for 24 hrs at 4°C and then transferred to 1x PBS. Tissue comprising the cervix, vagina and part of the uterine horns were embedded in paraffin and 5 µm thick longitudinal sections were cut. TUNEL staining (Promega DeadEnd Fluorometric

TUNEL kit) and Hematoxylin (HE) staining were performed by the Histo-Pathology Core at UT Southwestern Medical Center.

### **Immunohistochemistry**

Paraffin sections were deparaffinized using standard procedure. After antigen retrieval using sodium citrate buffer (10mM pH 6) for 20 mins at 4°C, sections were subjected to 0.5% hydrogen peroxide solution at RT for 20 mins (H1009, Sigma) in methanol to quench endogenous peroxidases. Sections were blocked with 10% normal goat serum (50062Z, Life Technologies) for 30 mins at RT and rinsed in 1x PBS. Subsequently, sections were incubated with streptavidin and biotin blocking kit (SP-2002, Vector Laboratories) for 20 mins at RT. After washing with 1x PBS the sections were incubated with primary antibody overnight at 4°C. The next day, slides were washed with 1x PBS and incubated with biotinylated secondary antibody for 1 hr at RT followed by VECTASTAIN ABC-HRP reagent, peroxidase (PK-7100, Vector Laboratories) for 30 mins followed by Vector NovaRED substrate peroxidase solution (SK-4800, Vector Laboratories) at RT. After rinsing the slides with tap water sections were counterstained using Hematoxylin (72804, Epredia) for 10 sec. Slides were washed in 1x PBS and dehydrated in 70% ethanol, 100% ethanol and Xylene. Finally, sections were covered with Cytoseal (8312-4, Thermo scientific) and dried for imaging.

### **Immunofluorescence**

Following deparaffinization and antigen retrieval as described above, tissue sections were blocked with 10% normal goat serum (500627, Thermo Scientific) for 30 mins at RT. Sections were rinsed in 1x PBS and incubated with primary antibody overnight at 4°C. The next morning, sections were washed in 1x PBS and incubated with secondary antibody for 30 mins at room temperature. Sections were mounted with Prolong Gold anti-fade reagent with DAPI (P36935, Invitrogen) and sealed with a coverslip.

### **In situ hybridization**

Chromogenic or Multiplex fluorescent RNAscope Kits (Advanced cell diagnostics 320511 or 323100) were used as per the manufacturer's instructions. Briefly, slides were deparaffinized in xylene, followed by rehydration in a series of ethanol washes. Subsequently, sections were heated in kit-provided antigen retrieval buffer for 15 mins and digested by kit-provided protease plus for 30 mins at 40°C (Advanced Cell Diagnostics) in a HybEZ hybridization oven (Advanced Cell Diagnostics). C2 and C3 probes were diluted in C1 probes at a 1:50 ratio and incubated on the slides for 2 hrs at 40°C. After each hybridization step, slides were washed two times at RT in a kit-provided 1x wash buffer for 2 mins. For chromogenic signals, hybridization signals were detected using diaminobenzidine (DAB). The RNA signal was identified as red punctate dots. For fluorescence signals, slides were mounted with DAPI and Prolong Gold antifade reagent (P36930) and sealed to dry and stored at 4°C until imaging.

### **Image analysis**

For Hematoxylin and immunohistochemistry, the whole slides were scanned using the Hamamatsu Nanozoomer 2.0 HT and viewed using NDP View2 software. For visualization of TUNEL, immunofluorescence and RNAscope data, images of longitudinal cervical sections were taken with Zeiss LSM780 inverted confocal microscope and Zeiss Axioscan Z1 digital slide scanner (Figures S2 and S3) with ZEN 3.0 (software) at 20x and 40x magnifications. To evaluate the temporal changes, all the fluorescent labeled images including opal dye used in RNAscope images were captured using the same detector gain and laser power using appropriate filter settings. The standard fluorescent filter wavelength settings used for immunofluorescent staining and RNAscope (opal dyes) are listed for excitation and emission wavelength respectively: DAPI (358/461 nm), FITC/ opal 520 (494/525 nm), Cy3/ opal 570 (550/570 nm) and Cy5/ opal 690 (676/694 nm). To compare the relative signal across time points, optimal imaging conditions for the time point with the lowest signal are applied to images at all time points and the captured images were rescaled linearly for each channel across all time points. Each individual image was processed with scale bars using Image J software.

### **Antibodies and probes**

Antibodies used for immunohistochemistry and immunofluorescence: rabbit anti-Keratin 10 (1:100, Abcam ab76318), mouse anti-IFITM1 (1:50, Proteintech 60074-1), rat anti-Ki67 (1:200, ThermoFisher scientific 14-5698-82), chicken anti-Keratin 5 (1:100, Biolegend 905901), Rabbit anti-Keratin 8 (1:100, Abcam ab53280), and Biotinylated goat anti-rabbit IgG (1:200, Vector laboratories BA-1000), goat anti-mouse IgG (1:200,

Vector laboratories BA-9200) and goat anti-Rat IgG (1:200, Vector laboratories BA-9400), Donkey anti-chicken Alexa Fluor 488 (1:600, Jackson ImmunoResearch 703-545-155), Goat anti-rabbit Alexa Fluor 594 (1:600, Thermo Fisher A-11012) conjugated secondary antibodies. Probes used for RNAscope (Advanced Cell Diagnostics): *Krt5* (415041), *Avil* (C1, 498531), *Dsg1a* (C2, 842861), *Spdef* (C2, PN 544421), *Muc5b* (C2, 471991), *Muc1* (C1, 421871), *Pigr* (C1, 552591), *Rbp2* (C3, 444091), *Olfm4* (C2, 311831).

### Ascending infection by vaginal *E.coli* inoculation

Live *E. coli* (serotype O55; ATCC) (20ul bacteria equal to  $10^5$  CFU) was inoculated into the vagina on the morning of GD16 as described previously.<sup>20</sup> After 24hrs of *E.coli* inoculation, pregnant females (HAKO and wild type) were sacrificed and one uterine horn was placed in PBS. The second uterine horn, cervix-vagina, fetal membranes, and placenta were flash-frozen and stored at  $-80^{\circ}\text{C}$ . The uterine tissue in PBS was gently vortexed to release bacteria into PBS. One ml of the PBS was spread on Luria-Bertani agar plates and incubated at  $37^{\circ}\text{C}$  overnight and the bacterial growth on the agar plates was documented. The frozen tissues were used to isolate RNA and measure gene expression of proinflammatory genes (IL-1 $\beta$ , TNF- $\alpha$ , IL-6, Mmp8) and Cx43 relative to housekeeping gene cyclophilin by qPCR.

### Single cell data clustering

Seurat V3.2 was used for scRNA-seq data analysis.<sup>92</sup> The standard workflow was used for clustering. First, UMAP clustering was performed on each time point individually. Then DoubletFinder V2.0.3 was used to identify any doublets. Cells that were identified as doublets were removed. After doublet removal, the cell type of each cluster was determined. The expected cell types include epithelial, stromal, endothelial, immune, and blood cells. Using known genes, all these expected cell types were found in the single-cell data. Any clusters that were not identifiable as a particular cell type were removed from the analysis. Generally, the removed clusters exhibited low gene counts and were of poor quality. Next, the following QC filters were applied:  $100 < \text{nFeature\_RNA} < 6,000$  (# of genes detected/cell),  $100 < \text{nCount\_RNA} < 10,000$  (UMI's detected/cell), and  $\text{percent.mt} < 20\%$  (mitochondrial contamination). After the data was cleaned, clustering was re-run using the Seurat pipeline at each time point. The clusters identified at each time point were used for further downstream analysis. Seurat functions, FindMarkers and FindAllMarkers, were used to identify differentially expressed genes between clusters. scVelo 0.2.2 was used for RNA velocity analysis after clustering was performed. We initially tested multiple approaches for batch effect correction. But these approaches introduced significant bias, and independent spatial analyses only confirmed the clustering results that lacked batch correction. One explanation is that batch correction ideally works on samples where a set of invariant cells can be anchored. However, batch correction is incompatible with dynamic samples in this study where each time point exists in a unique hormonal signaling environment.

### Single nuclei ATAC-Seq data analysis

ArchR 2.0 was used to analyze the snucATAC-seq data.<sup>42</sup> The cells from each time point were filtered using a TSS enrichment score cut-off above 4 and a unique nuclear fragments cut-off above 1000. Doublets were also identified and filtered using the AchR workflow. After filtering and doublet removal, each time point NP, day 6, 12, 15, 18, and IL had 3288, 7806, 5824, 6530, 2312, and 4998 cells respectively. Cells from all time points were clustered using UMAP, and gene scores and deviation scores were calculated using the standard ArchR workflow. Cell type identity for each cluster was determined using the gene score for known genes, and those used in the scRNA-seq data analysis.

## QUANTIFICATION AND STATISTICAL ANALYSIS

For gene expression measurement in the ascending infection mouse studies, differences in gene expression between the reproductive tissues collected from HAKO and wild type were analyzed by Microsoft Excel software. A 2-tailed ratio-paired Student's *t*-test was performed using the average  $\pm$  SEM. Differences with a *p* value  $< 0.05$  were considered significant. Pooled data from  $N = 6$  mouse tissues/genotype/treatment are shown.

Software. For staining by immunohistochemistry, immunofluorescent and RNAscope, data were processed by Fiji/ImageJ software downloaded from the U.S National Institutes of Health website.